Universidade de Aveiro Departamento de Electrónica, Telecomunicações e Informática,
2015

Tiago Sousa Moura

Sistema eficiente de recolha de energia resultante do espectro da D-TV

(High-efficiency energy harvesting system from D-TV spectrum)

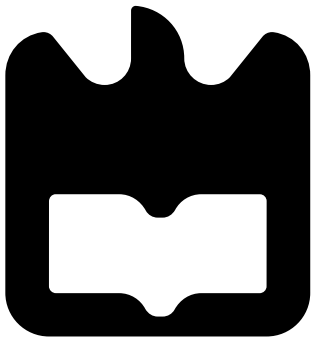

Tiago Sousa Moura

Sistema eficiente de recolha de energia resultante do espectro da D-TV

(High-efficiency energy harvesting system from D-TV spectrum)

Dissertação apresentada à Universidade de Aveiro para cumprimento dos requisitos necessários à obtenção do grau de Mestre em Engenharia Electrónica, realizada sob a orientação científica do Dr. Nuno Borges de Carvalho, Professor Catedrático com agregação do Departamento de Electrónica da Universidade de Aveiro e co-orientação do Dr. Pedro Pinho, Professor Adjunto com agregação do Instituto Superior de Engenharia de Lisboa.

Aos meus pais e irmã, pela oportunidade e esforço que fizeram para que chegasse até aqui.

o júri / the jury

presidente / president

Prof. Dr. Rui Escadas Martins
Professor Auxiliar da Universidade de Aveiro

vogais / examiners committee

Prof. Dr. Nuno Borges de Carvalho
Professor Catedrático da Universidade de Aveiro

Prof. Dr. Rafael Caldeirinha
Professor Coordenador da Escola Superior de Tecnologia e Gestão de Leiria

agradecimentos / acknowledgements

Começo por agradecer aos meus colegas e amigos, àqueles que me acompanharam desde o início nesta longo percurso académico e um especial obrigado aos que acompanharam mais de perto o presente trabalho, contribuindo com motivação, sugestões e correções. Um muito obrigado aos meus orientadores, Prof. Nuno Borges de Carvalho e Prof. Pedro Pinho, por toda a disponibilidade e paciência demonstrada para comigo e pelo esforço que fazem para fazer do Instituto de Telecomunicações um local propício ao desenvolvimento ciêntifico, que contribui para o sucesso dos alunos. Aproveito também para agradecer no geral aos colaboradores do Instituto de Telecomunicações que auxiliaram este trabalho das mais diversas formas. Por fim, um muito obrigado à minha grande família e aos amigos de sempre, por terem acreditado em mim e me terem ajudado a chegar até aqui.

palavras-chave

Colheita de energia, baixa potência, eficiência, televisão digital, transmissão de energia sem fios, rectificadores, díodo Schottky

resumo

A recolha de energia do meio ambiente para alimentar dispositivos como forma de os tornar auto-sustentáveis tem vindo cada vez mais a suscitar interesse. Por outro lado, o crescimento contínuo do espectro resultante das telecomunicações constitui uma grande oportunidade para a colheita de energia. Assim sendo, neste trabalho é proposto um sistema altamente eficiente de recolha de energia de rádio-frequncia que utiliza o sinal da televisão digital (D-TV) portuguesa e que converte-o em tenso que poderá ser reaproveitada. De forma a ser vantajoso, o sistema é otimizado para operar a baixos níveis de potência. Assim, o presente trabalho pretende também fornecer orientações para o correto desenvolvimento do sistema de colheita de energia para baixa potência de entrada, contribuindo para o desenvolvimento de projetos futuros.

O sistema é dividido numa antena recetora e num retificador. Para o retificador são propostas três soluções distintas: um díodo série, um díodo paralelo e um duplicador de tensão. A eficiência obtida é semelhante para as três configurações - cerca de 54% para um sinal de entrada sinusoidal com um nível de potência de -10.5 dBm. Medições com o multiplicador de tensão e o sinal real da D-TV como entrada mostraram uma eficiência de 63% para o mesmo nível de potência. Relativamente à antena, é proposta uma *patch* com *slots* e com um elemento parasita que utiliza como substrato dielétrico FR-4. Esta configuração resulta da necessidade de melhorar a largura de banda da *microstrip* simples. Medições mostraram um aumento da largura de banda em cerca de 4 vezes quando em comparação com uma *patch* simples.

keywords energy harvesting, low-power, efficiency, digital television, wireless power transmission, rectifiers, Schottky diode

abstract Collect energy from the surroundings is being biased to power-up devices in order to turn them self-sustainable. On the other hand, the spectrum resultant from the telecommunications tends to progressively increase and becomes wide-reaching, constituting an enormous opportunity to energy harvesting. Thus, in this work a high efficiency radio-frequency energy harvesting system is proposed that takes uses of the Portuguese Digital Television (D-TV) signal to obtain Direct Current (DC) power. To be useful, the system is optimized to operate at low power conditions. So, this work also aims to provide reliable guidelines in the design of energy harvesting systems with low-input power.

The system is divided into an antenna and a rectifier. For the rectifier, three different solutions are presented: a single-series diode, a single-shunt diode and a voltage doubler configuration. The efficiency is similar for the three rectifiers – around 54% with a sine-wave excitation and -10.5 dBm input power. Field measurements with the voltage doubler has proven 63% efficiency for the same input power. As receiver antenna is proposed a slotted patch with a stacked parasitic based on FR-4 substrate. This configuration results from the need to improve the bandwidth of the basic microstrip patch. Measurements have proven and enhancement around 4 times in comparison with a basic patch.

Contents

List of Figures

List of Tables

Acronyms

ADS	Advanced Design System
ANACOM	*Autoridade Nacional de Comunicações*
BW	Bandwidth
CST	Computer Simulation Technology
DCS	Digital Cellular Service
DC	Direct Current
D-TV	Digital Television
EH	Energy harvesting
EM	Electromagnetic
ERP	Effective Radiated Power
EIRP	Effective Isotropic Radiated Power
FET	Field Effect Transistor
GSM	Global System for Mobile communications
LPF	Low-Pass Filter
MMDS	Multichannel Multipoint Distribution Service
MoM	Method of Moments
MPT	Microwave Power Transmission
PAPR	Peak-to-Average Power Ratio
PLF	Polarization Loss Factor
QPSK	Quadrature Phase-Shift Keying

RF	Radio-Frequency
RFID	Radio-Frequency Identification
SA	Spectrum Analyser
SG	Signal Generator
SPS	Solar Power Satellite
TDT	*Televisão Digital Terrestre*
TV	Television
UHF	Ultra High Frequency
UMTS	Universal Mobile Telecommunications System
VNA	Vector Network Analyser
VSWR	Voltage Standing Wave Ratio
WiFi	Wireless Fidelity
WPT	Wireless Power Transmission
WSN	Wireless Sensor Network

Chapter 1

Introduction

1.1 Motivation

The need to explore alternative renewable energy had become an important focus nowadays due to the scarcity of fossil fuels required to produce electrical energy. The high levels of pollution caused by the use of these fossil fuels are also a concern to the environment and future of humanity. Moreover, the life-time of the batteries portable devices and the pollution and health risks as consequence of their deposition are also problems to be solved.

Regarding the batteries life-time, the main ambiguous problem are the wireless sensors. In many cases, recharging or replacing the sensors batteries could be difficult, costly or even impossible dependently of their location. Sensors implanted on structures to evaluate their corrosion or in the human body for medical applications are two examples of complex sensors locations where the replacement of batteries isn't suitable.

Also, the autonomy of the gadgets is circumscribed by their battery, requiring the need to be quite often recharged, which limits the devices portability. Due to increased dependence towards these gadgets in quotidian life, improvements or solutions for the battery life-time issues are highly desired.

The Radio-Frequency (RF) Energy harvesting (EH) consists in capturing electromagnetic power from RF signals available in the surroundings and converting it into power that can be reused. The increase of sources that radiate considerable amounts of power, such as cell phone towers, WiFi, broadcast television signals, etc., induces a global spread of the available electromagnetic fields in the air. Therefore, RF EH constitutes a solution for the previously mentioned problems. Other examples of EH sources are the solar radiation, vibration, wind and thermal gradients. For example, in contrast with the solar radiation or wind, the electromagnetic fields resulting from the telecommunications is a continuous source of power, during day and night and independent of the weather conditions.

1.2 Objectives

The general purposes of this work are study, design and validate an RF EH system responsible for collecting electromagnetic energy from the Portuguese D-TV and then transform it into DC power that can be reused to feed other devices.

This system should be able to successfully operate at low incident power conditions, due to the limited RF power that is possible to obtain from the available spectrum opportunities. The performance key parameter along this work is the conversion efficiency. Higher conversion efficiencies increase the range relative to the transmitter where is possible to take use of the EH system. In addition, the receiver antenna is also responsible to improve the system range. In this case, antenna gain plays an important role. Hence, this work has also as goal to achieve improved performance to low incident power levels, aiming to obtain an enhancement relative to the stated in the literature. Besides performance, another objective is to obtain a low cost system.

Moreover, this dissertation intends to contribute with a know-how in the EH system design, presenting the considered steps to take into account in order to obtain the improved performance as mentioned above and contribute for future works.

1.3 Outline

This dissertation is organized as follow:

- Chapter 2 provides the majority background required to the work development. Essentially, it presents a system overview, where each block is briefly analysed. Also, the Portuguese D-TV is introduced as RF source power for the EH system, according to the spectrum opportunities. Finally, different work in the field reported in literature is summarized.

- Both Chapter 3 and Chapter 4 focus on the rectifier – the main core of this work. Chapter 3 pretends to provide the theoretical concepts involved in the rectifier, namely the Schottky diode as non-linear element and the working process of different rectifier topologies. Moreover, a simulation study is made to consolidate the theoretical exposure. Chapter 4 provides the rectifier design procedures made with the Advanced Design System (ADS) software and the simulations and measurements results are presented and analysed.

- In Chapter 5 the receiver antenna is exposed. First, some briefly theoretical concepts are endorsed and then the design steps are presented according to the system requirements. The simulations are made with the Computer Simulation Technology (CST) software.

- Chapter 6 validates the EH system with field measurements around a Portuguese D-TV transmitter being exhibited. The results are analysed according to some different factors in each measure.

- Finally, in Chapter 7 conclusions are withdrawn, summarizing the main achievements reached along the project. Also, in order to continue the developed work, some prospective directives are suggested.

1.4 Contributions

Within this work were developed two articles. The first, entitled "Parasitic Stacked Slot Patch Antenna for DTT Energy Harvesting", was accepted at the IEEE AP-S Symposium on Antennas and Propagation and URSI CNC/USNC Joint Meeting, that will be held on July 2015 at Vancouver. The second, "High-Efficiency D-TV Energy Harvesting System for Low-Input Power", was submitted to the Wireless Power Transfer journal released by Cambridge University Press.

Chapter 2

State of the Art

2.1 Wireless Power Transmission

2.1.1 Historical Background

Wireless Power Transmission (WPT) systems use the air as via for transferring energy between two separate nodes. The concept began in the 19th century first with the work of Heinrich Hertz and later than with Nikola Tesla. Considered the "Father of Radio", Tesla was responsible for the first demonstration of wireless communication. He builds a coil connected to a mast with a copper sphere at its top in order to transmit energy. Although there is no record that indicates if it was collected any energy, his discovery let him state in his patent that "becomes possible to transmit through easily-accessible and only moderately-rarefied strata of the atmosphere electrical energy"[5].

Later, now in the 20th century, H. V. Noble conduct another experiment. This time two identical dipoles were used, one as transmitter and another as receiver, which allowed collecting hundred of watts.

The progress made during the World War II, such as the developments in the radar technology, has defined the modern concept of WPT. Since the 1950s, W. C. Brown has been researching the rectification of microwave signals with the advancement of high-power microwave tubes by Raytheon Company. In fact, Brown was responsible of the rectenna concept and develops the first one in the early 1960s to power a model helicopter by wireless power transmission [6]. The diodes used until then in the rectifiers were point-contact diodes. The usage of Schottky barrier diodes allowed, in the following years, the emerging of rectenna devices with higher efficiencies. In 1977, Brown reports a 90.6% efficiency rectenna with an input power of 8W and aluminium bars in the dipole antenna [7]. Later, a 85% conversion efficiency with thin-film rectenna at 2.45 GHz was developed [8].

The Solar Power Satellite (SPS) and the Radio-Frequency Identification (RFID) were the two main research topics that significantly contribute to developments in the transmission of wireless power. Two main differences distinguish the SPS from the RFID: while SPS demands great distances and high level powers, RFID focus in smaller distances and

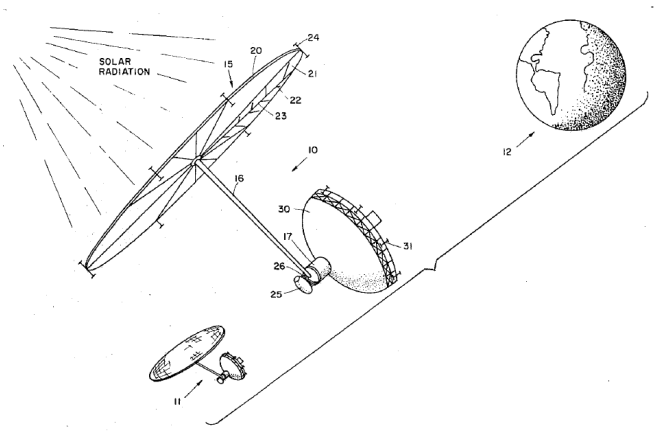

Figure 2.1: SPS system [1].

much lower power (under 1 Watt).

The SPS, proposed by P. E. Glaser in 1968, is a mean of exploiting solar radiation, where the solar energy would be collected using large solar panels placed in the orbital satellites and then it would be beamed to the Earth through microwave power transfer [1]. In the following years was proven the feasibility of the SPS, although it stills in the experimental stage nowadays.

The RFID has been profoundly studied and the majors applications are tracking – via battery-less RFID tags – and backscatters sensors. Other recent WPT systems supported on RFID technologies have been studied, e.g. bio-implanted sensors in human body for electrocardiogram and other medical control applications [9].

2.1.2 Theoretical Concepts

The main difference between a communication and a WPT system relies on the efficiency. Typically, the efficiency achieved with the former is low, but sufficient to address the data transfer. In turn, the WPT aims high efficiency [10]. The WPT can be divided into two main categories: near-field and far-field. Inductive and resonant coupling are two techniques employed in near-field category, as the RFID. This techniques consists in the same fundamentals as transformers. Although they are efficient mechanisms for WPT, the rapidly decrease of the coupling between the transmitter and receptor with distance leads to a short range where is possible to effectively transmit the power.

One the other hand, the SPS system is an example of a far-field WPT. Into far-field WPT, one widely used technique is the Microwave Power Transmission (MPT). The efficiency of the transmitted power can remain with acceptable values for a long range distance between the transmitter and the receiver node.

An MPT system is presented in Figure 2.2. The transmitter, in the left, is responsible for generate the RF signal with a certain frequency and power, $P_{RF,t}$. Then, the transmitting antenna, with a gain G_t, radiates the power through the free space. The transmitted

power must follow the rules imposed by the regulatory identities[1]. In turn, the receiver node, in the right, is responsible for collecting the signal through the receiver antenna (with gain G_r) and then the rectifier transforms the received RF power ($P_{RF,r}$) into DC power. In the MPT system, the receiver plays an important role. The rectifier circuit integrated with an antenna is commonly recognized as rectenna.

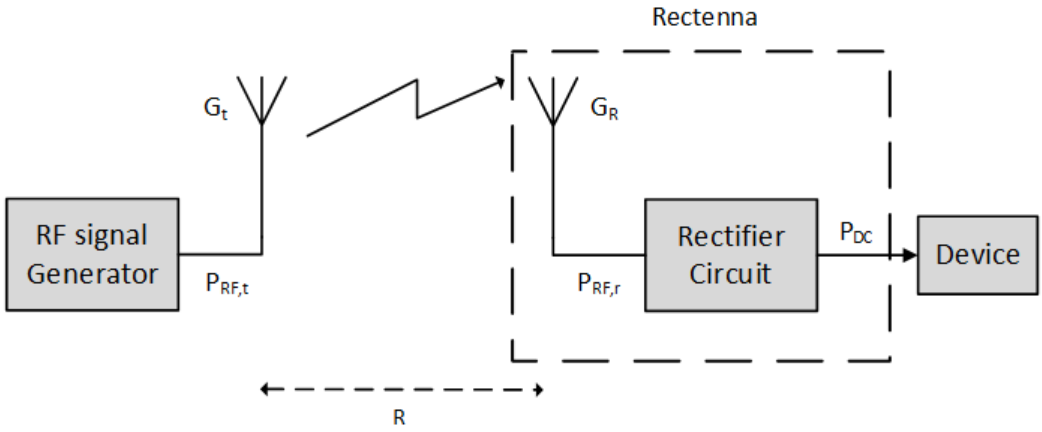

Figure 2.2: A MPT system – block diagram.

The Equation 2.1, known as the Friis transmission equation, allows the evaluation of the free space path loss effect in the receiver power [11]. This states that, under ideal conditions, the ratio between the received power (P_r) and transmitted power (P_t) is

$$\frac{P_{RF,r}}{P_{RF,t}} = G_t G_r \left(\frac{\lambda}{4\pi R}\right)^2 \tag{2.1}$$

where R is the distance between antennas (according to Figure 2.2) and λ is the wavelength of the transmitted signal. According to this equation it is possible to conclude that the free-space path loss is proportional to the square distance R and then, a small variation in the distance between the antennas leads to considerable changes in the received power.

Moreover, reorganizing Equation 2.1, it can be seen that received power is proportional to the product $G_t P_t$. In turn, this product is characterized as Effective Isotropic Radiated Power (EIRP). Therefore, the received power, in dBm, can be expressed as shown in Equation 2.2, as follow:

$$P_{RF,r(dBm)} = EIRP_{dBm} + G_r + 20log_{10}\left(\frac{\lambda}{4\pi R}\right) \tag{2.2}$$

[1]In Portugal the regulator identity is *Autoridade Nacional de Comunicações* (ANACOM)

2.2 Energy Harvesting System – Overview

The EH system assents in the same fundamentals as MPT. However, instead of dedicated transmitters sources radiating high amounts of energy, the EH make use of the available spectrum induced by the radio communications. Therefore, the available power at the receiver node is typically much smaller than in an MPT system. The low input power levels is the main challenge regarding the design of an EH system, because the response of the system must be improved to these power levels.

The EH system is the aggregation of various blocks, typically: matching network, rectifier circuit and low-pass filter. This system is shown in Figure 2.3. A detailed explanation of each block is presented below.

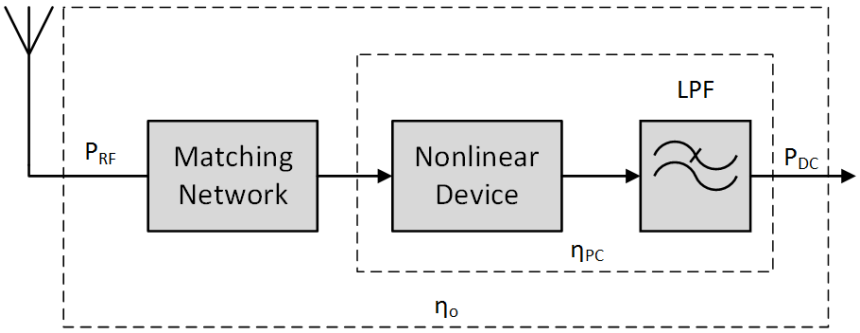

Figure 2.3: Rectenna – block diagram.

Receiver Antenna

The electromagnetic energy in the surroundings is collected through the receiver antenna. An wideband antenna with high gain should be considered to increase the system performance. As examples of antenna configurations are the dipole, YagiUda, microstrip patch or parabolic dish and so on [12].

Matching Network

The matching network prevents the reflections between antenna and the non-linear device. Thus, under ideal conditions, all the energy collected will be utilized to produce the DC power. In other words, the matching promotes the impedance adaptation between the antenna and the rest of the circuit. Considering an antenna with the input impedance of $R+jX$, the input impedance of the rectifier required to promote the matching is $R-jX$, the complex conjugate of the antenna input impedance.

Non-linear Element

The non-linear element is responsible to convert the RF into DC power. The most common element employed in the rectification process is the Schottky diode, due to the lower

voltage drop and faster switching time. Note that instead of a single non-linear element, a combination of two or more elements is also possible. According to this combination the rectifier is associated with a topology.

Low-Pass Filter

The Low-Pass Filter (LPF) at the end of the circuit is responsible to block all the RF signal and provide only the DC component, desired to feed the device or charge a battery.

2.2.1 Efficiency

Efficiency is usually the most important figure of merit in EH systems and allows the quantification of the power losses along them. The mismatch between the antenna and rectifier and the non-linear device(s) of the rectifier are the main contributors to the losses within the circuit.

Defining the desired DC output power as P_{DC} and the available power at the input of the rectifier as P_{RF}, the overall efficiency η_o is defined as 2.3 and take into account the losses due to the impedance mismatch and the losses in the non-linear device.

$$\eta_o = \frac{P_{DC}}{P_{RF}} = \frac{V_{DC}^2}{R_L \times P_{RF}} \tag{2.3}$$

The power conversion efficiency η_{PC}, is a metric of the rectifier which discards the reflected RF power, $P_{reflected}$, due mismatching between the receiver antenna and the rectifier. Therefore, η_{PC} is the ratio of the DC output power and the power that is actually delivered to the rectifier, as present in Equation 2.4. In this case, the main evaluation of the power conversion efficiency is the losses in the non-linear device(s).

$$\eta_{PC} = \frac{P_{DC}}{P_{RF} - P_{reflected}} \tag{2.4}$$

Only a perfect matching between antenna and rectifier allows η_o to be equal to η_{PC}, otherwise η_o is always lower. The overall efficiency provides a more accurate figure of merit of the RF EH system. Hence, along the developed work is adopted the overall efficiency, unless otherwise is stated.

Besides the improvements in the receiver, another way to boost the rectifier efficiency is to transmit a proper RF signal. The use of multi-sine signals with high Peak-to-Average Power Ratio (PAPR) had proven to be feasible for this effect [13]. The performance increase of the Schottky diodes when excited with high PAPR is explained in [14].

2.3 Spectrum Opportunities

As mentioned before, there are several spectrum opportunities that are possible to use as source for RF EH. To evaluate and obtain reliable information regarding the spectrum opportunities, measurements at Aveiro city (Portugal) were performed. This measurements,

presented in Figure 2.4, were made from 200MHz to 3 GHz with a Rohde & Schwarz FSH8 Spectrum Analyser (SA) connected to the wideband HL300 antenna. Additionally, it should be noticed that the referred spectrum was measured at an outdoor environment.

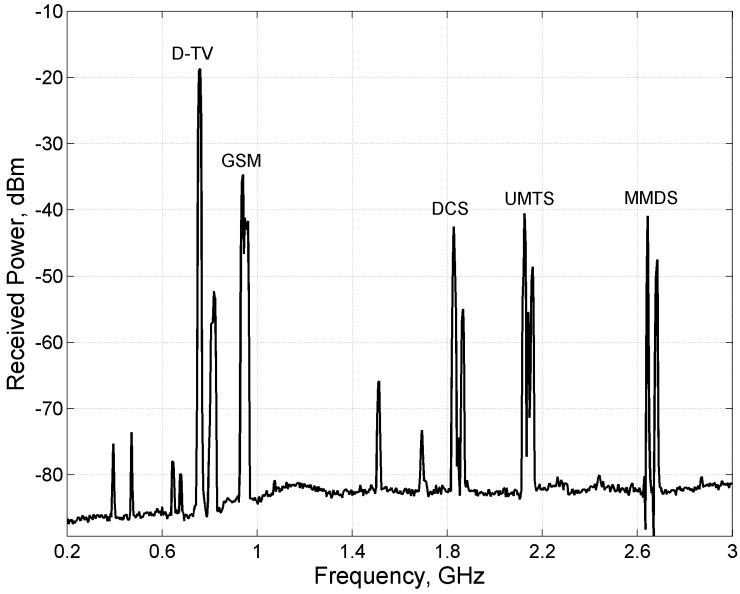

Figure 2.4: Power spectrum at Aveiro city.

Among others, the following spectrum opportunities are clear identifiable [15]:

- D-TV – 750 to 758 MHz;
- GSM – 925 to 960 MHz;
- DCS – 1805 to 1880 MHz;
- UMTS – 2110 to 2170 MHz;
- MMDS – 2500 to 2690 MHz;

The D-TV is the broadcast Portuguese Digital Television and Multichannel Multipoint Distribution Service (MMDS) is mainly used for satellite television broadcast as an alternative for the cable television. The Global System for Mobile communications (GSM), Digital Cellular Service (DCS) and Universal Mobile Telecommunications System (UMTS) are mobile communications systems. The GSM is also known as GSM-900 and the DCS as GSM-1800.

Despite the wide spectrum opportunities along the measured frequency band, the D-TV clearly exhibits a higher power density, explained by the close proximity to a D-TV transmitter.

2.3.1 Portuguese Digital Television

The Portuguese D-TV, also known as *Televisão Digital Terrestre* (TDT), starts in Portugal in 2009 as result of the analog signal switch-off, established to occur by the European Commission in 2012. TDT allows a more accurate electromagnetic spectrum efficiency, where the same bandwidth is able to broadcast more TV channels. Therefore, a percentage of the spectrum occupied by analogue TV is now free to another utilities [16]. Also, the digital broadcast permits more quality transmission, without suffering the multipath effects that occurs in analogue transmission.

Portugal has 257 transmitters radiating in 8 different channels and disperse in way to cover all the country with the D-TV signal, as exhibited in Figure 2.5. Table 2.1 presents the number of transmitters in each channel and is evident that the majority of transmitters radiate at channel 56 operating from 750 to 758 MHz. The Effective Radiated Power (ERP) of the transmitters at channel 56 has typical values from 6.5 W up to 8600 W [17].

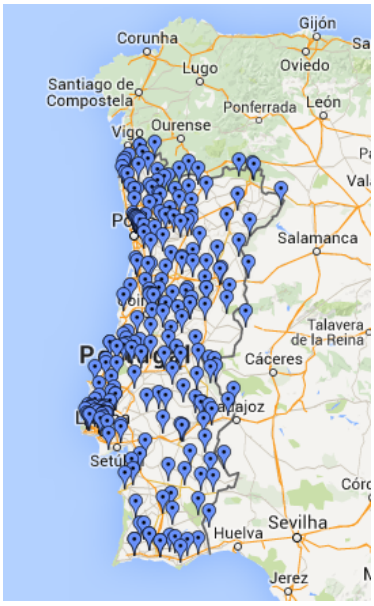

Figure 2.5: Location of the D-TV transmitter in Portugal.

In Aveiro city is located a D-TV broadcast tower at 40°38′33.38″N latitude and 8°39′ 8.52″W longitude. This transmitter is at the heart of the city, where there is a high population density, and radiates 3200 W of ERP.

Using Equation 2.2 it's possible to estimate the received power for a certain distance from the transmitter. Thus, in Figure 2.6 is presented the location of the Aveiro central D-TV transmitter and also the expected received power for different distances. For example, for a distance between transmitter and receiver of 200 meters, the received signal is approximately -11 dBm. To this evaluation, a receiver antenna with no gain was considered, which is a rudely approximation, however it works as a simple estimation.

As expected, is proved that the more transmitter and receiver are close, the higher is

Channel	Freq (MHz)	Number of Transmitters
56	750-758	231
55	742-750	2
54	734-742	11
49	694-702	4
48	686-694	3
47	678-686	3
46	670-678	2
42	638-646	1
Total		257

Table 2.1: Number of D-TV transmitters in each channel.

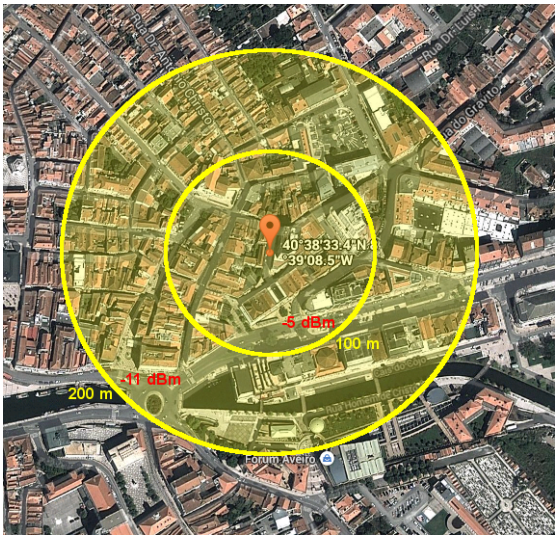

Figure 2.6: Aveiro D-TV transmitter location and power versus distance according to Friis Transmission equation.

the received power. Thus, energy harvesting nearby an transmitter assumes a even more useful role, specially in a high density population, as the Aveiro city case.

Additionally and as conclusion, according to the spectrum opportunities analysis and the following exposure regarding the Portuguese D-TV, it constitutes one of the most interesting RF power sources for harvesting, due to the high transmitted power levels, high number of sources, which make it wide-reaching.

2.4 Low Incident Power Rectification – Literature Review

The first reported low-power density rectenna date to 1991, that was able to rectify a power density level that was "10000 times lower than those normally used" ($5\mu W/cm^2$) operating at 2.45GHz [18]. In this design the diodes were used at a power level capable of maximize their efficiency. The collecting element adopted was a broadside array (48 dipole) to achieve high efficiencies at low-power densities. The efficiency reached was about 50%.

Nowadays, the developments made in the Schottky diodes, as well as other non-linear elements, and the improvements of other technologies, such as the simulation tools, allowed new challenges and higher conversion efficiencies.

The importance of efficiency was already mentioned before and will be used to evaluate the rectifiers state of the art further ahead. However, considering only efficiency can be a tricky analysis due to the following reasons:

- Rectifier efficiency depends strongly in the input RF power density and rectifiers are likely more efficient at higher input power levels. Thus, efficiency should always be referred to the input power;
- The definition of efficiency could be responsible for disagreements. For example, sometimes is not clear if the efficiency refers to the overall efficiency (η_o) or to the power conversion efficiency (η_{PC}), as distinguished previously in Section 2.2.1;
- Frequency of operation is also responsible for different performance analysis. Different matching networks are required if rectifier is intended to be a single band, a multi-band or broadband rectifier. These multi-band and broadband networks usually have lower quality factor than single frequency matching networks, which reduces the system efficiency [19];

Therefore, the rectifiers should not be directly compared based only in their efficiency and these considerations were taken in Table 2.2, that presents some rectification works reported in literature and the respective performances. Additionally, Table 2.2 focuses in devices that are able to operate at low incident power, considering only the reported work with performance evaluation below 0 dBm.

In [20] is proposed a two stage voltage multiplier employing SMS7630 Schottky diodes as non-linear element. This work has also shown that modulated signals (QPSK in this particular case) induces higher conversion efficiency than single-tone signals, due to a certain PAPR. The receiver antenna is a patch with cross shaped slot to reduce dimensions and provide a dual linearly polarization with 7.5 dBi gain. The rectifier is directly connected at the bottom of the antenna, resulting in a compact rectenna. However, efficiency is measured based in the estimation of the input power presented to the rectifier.

The rectenna presented in [2] is an antenna directly matched to the rectifier input, avoiding the matching network, as shown in Figure 2.7, and was able to reach 75% efficiency. The HSMS-2850 Schottky diode is used as non-linear element.

Frequency (GHz)	Input RF Power	Efficiency	Reference
2.45	-10 dBm	42%	[20]
2.45	-10 dBm	75%	[2]
0.45	-11.5 dBm	40%	[21]
1.8	-5 dBm	50%	[3]
2.45	-10 dBm	60%	[22]
0.85/1.85	-20 dBm	15/15%	[23]
0.55	-15 dBm	30%	[24]

Table 2.2: Performance of the rectennas or rectifiers reported in the literature.

The RF-to-DC converter presented in [21] is a series diode configuration, also with the SMS7630 Schottky diode. The single-tone measurements exhibits around 40% efficiency at -11.5 dBm input power. Furthermore, is also proved the efficiency improvements with a chaotic waveform as input signal. In this case, an efficiency around 60% is obtained with the same input power. Still, the RF-to-DC converter is directly connected to the generator and there are no experiments with the rectifier connected to an antenna.

In energy harvesting the input power can change substantially. Thus, in [3] is proposed a approach to avoid the "well-defined" rectifier operating point. The proposed device is able to adapt itself according to RF input power level and then assuring an improved performance within a large range of input power (-30 to 30 dBm). This is made with the combination of three different rectifier topologies optimized to operate at different power levels: the series diode, the shunt diode and the bridge rectifier. The Schottky diodes employed in each rectifier were, respectively, the HSMS-2850, the HSMS-2860 and the HSMS-2820, all from Avago. Figure 2.8 shows the experimental prototype developed. Regarding the low input power levels, the maximum efficiency is around 50% between -5 and 0 dBm with the series diode configuration, as reported in Table 2.2. At higher input power levels, the shunt diode rectifier reaches 70% at 15 dBm and the bridge presents the higher efficiency – 78% at 23 dBm. It is then clear with this work that both series and shunt configurations have better performance at lower input power levels than bridge rectifier.

The rectifier proposed in [22] is another series diode configuration and use the HSMS-2855 Schottky diode. This work, demonstrate the efficiency improvements with a resonance effect, adding a microstrip line that, along with the filter capacitor, is able to cancel the imaginary component of the diode impedance.

The dual-band series diode rectifier suggested in [23] is the one with lower efficiency shown in Table 2.2. However, it should be noticed that the input power is also the lower and, for this reason, its reasonable a lower efficiency. Additionally, being a dual-band network it has a lower quality factor and reduces the efficiency, as mentioned previously.

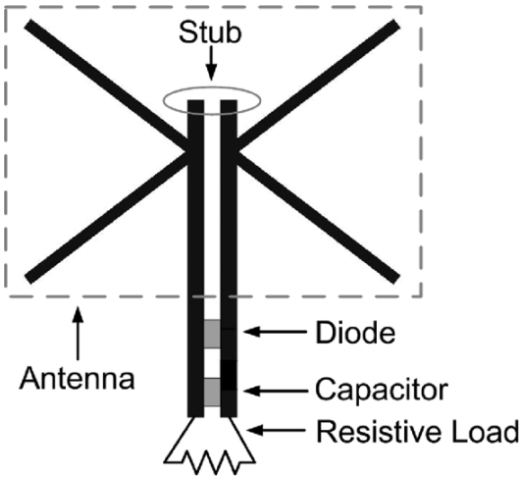

Figure 2.7: Rectifier antenna proposed in [2].

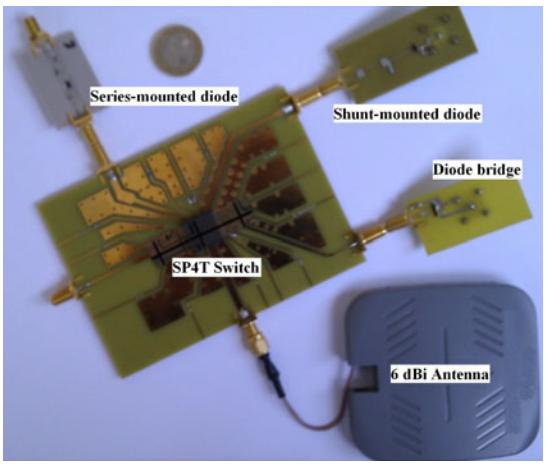

Figure 2.8: Experimental prototype presented in [3].

The SMS7630 Schottky diode is used in this work.

Relative to the last entry of Table 2.2, the key was the high bandwidth of the rectenna. Despite not mentioned the adopted non-linear element, the rectifier in [24] is again a basic series diode topology. The singularity of this system is the matching network tunable capability to two different bands, resulting in a wideband system. The antenna is a microstrip patch.

After this analysis into the low-power rectennas or rectifiers, it should be noticed the unanimous choice regarding simple rectifier topologies, as well the widely employed SMS7630 or HSMS-2850 Schottky diodes in most of the referred works. There are many other works regarding rectennas, however only a few of them have demonstrated considerable performance at low input power levels. Therefore, according to this analysis is clear that low-power rectification is still an open issue.

Chapter 3

Rectifier Circuit Analysis

The main core of this project is the rectifier circuit, responsible to convert the RF into DC power. Therefore, the goal of this chapter is analyse the rectifier and its elements, to create a bridge for the rectifier design shown in Chapter 4.

The Schottky diode is the non-linear element used in this project. As the key for the rectification, the chapter begin with the Schottky diode analysis to support its function understanding. Besides the referred importance, it is proved along the chapter that Schottky diode non-linearities are responsible for shaping the efficiency response to the input power.

This chapter also focuses on some of the many rectifier topologies options, exposing and analysing the concept of each one and differences among them. Hence, it aims to evaluate the configurations that better fulfils an EH system.

To complete this chapter, a simulation survey is made and analysed to consolidate the theoretical approach into the rectifier circuit. First, according to a commercial Schottky diode Spice parameters, is evaluated its non-linearities effect into the rectifier conversion efficiency. Second, is compared the performance of some commercial Schottky diodes. Finally, are studied the rectifiers topologies exposed in the theoretical analysis. This survey is made with ADS electronic design software.

3.1 Diode as Non-linear Element

There are different diodes classified according to its physical characteristics. The most common is the semiconductor pn-junction diode, where the n-type side contains the electrons and the p-type the holes.

The diode controls the current-flow and, ideally, it only flows in one direction. Thus, the ideal diode acts has a open or a short circuit. However, there are no ideal diodes in practice. The typically current-voltage characteristic of an semiconductor diode is presented in Figure 3.1 and has three different operation regions according to its terminal voltage, namely:

- Breakdown – diode operates in the breakdown region for reverse voltages lower than

the breakdown voltage (B_V). In this region a small increase in reverse voltages produces a large current increase in the reverse direction and could be destructive if the power dissipation limit is reached.

- Reverse – for negative voltages higher than B_V. It has a quite small current flowing in the reverse direction, mainly due to leakage effects and it increases with temperature rise.
- Forward – diode is forward-biased when its terminal voltage is positive and conduct the current in the forward direction. However, it is almost null until the threshold voltage V_t is reached. Both V_t and B_V voltages are intrinsic values of each diode.

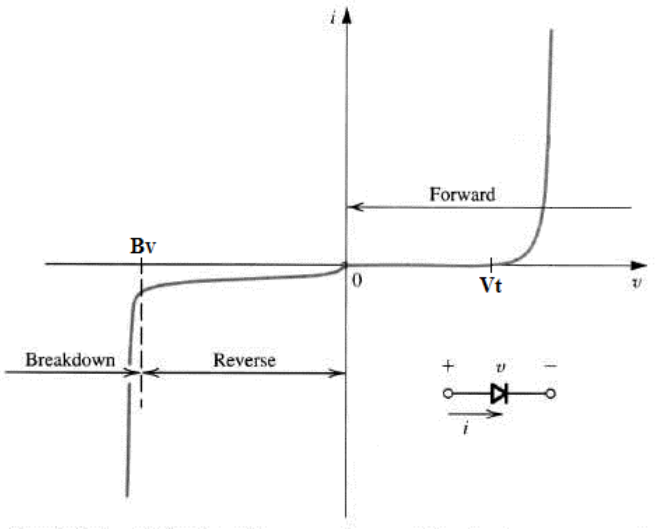

Figure 3.1: Typically i-v diode characteristic curve.

In Equation 3.1 is expressed the relation between the current flowing through the diode (I_D) and the voltage across it (I_D) for a junction diode,

$$I_D = I_S(e^{\frac{q}{nkT}V_d} - 1) \tag{3.1}$$

where I_S is the saturation current, q is the charge of an electron, n is the ideality factor, k the constant of Boltzmann and T the temperature [11].

Into the wide reaching diode applications, rectification is one of them. In fact, there are other non-linear elements that are able to rectify, however diode is widely employed in rectification design.

3.1.1 Schottky Diode

Unlike the classic pn-junction, Schottky diode consists on a metal-semiconductor junction. This junction allows a lower built-in voltage V_{bi} than conventional diodes (usually in

the range 0.2 0.5 V). Also, the switching of the Schottky diode from the conducting to the non-conduction state is faster than the pn-junction diode. All the differences pointed so far make the Schottky diodes the correct choice for various applications, including rectification, particularly at higher frequencies and at lower input power levels. This also explains the widely employ of this diodes in the literature, as shown in Section 2.4.

However, being a non-linear element it demands a careful analysis into its non-linearities to evaluate their influence in the conversion efficiency.

A typically equivalent Schottky diode model when forward-biased is exhibited in Figure 3.3. R_S is the series resistance, C_j and R_j are the junction capacitance and resistance, respectively. Additionally, the model should include some packaging parasitics to obtain a more accurate approximation to the practical diode behaviour. However, these are not considered to simplify the analysis. Also, to understand the origin of the intrinsic non-linearities, Figure 3.2 presents a typical diode cross-section [25].

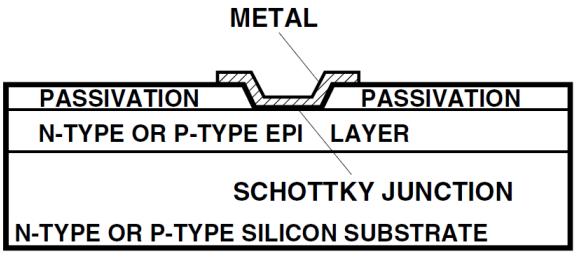

Figure 3.2: Schottky diode cross-section.

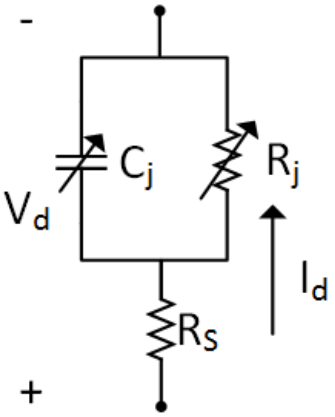

Figure 3.3: Typically Schottky diode model.

The junction capacitance, C_j, can be ignorable at low frequencies, although for higher frequencies (a few MHz) its effect becomes significant [26]. This capacitance is highly affected by the junction dimensions, namely, the diode contact and epitaxial layer (Figure 3.2) and it changes according to the input power. The junction capacitance can be computed by the approximation expressed in Equation 3.2,

$$C_j = C_{j0}\left(1 - \frac{V_0}{V_{bi}}\right)^{-M} \tag{3.2}$$

where C_{j0} is the diode zero-bias junction capacitance, V_0 the output DC voltage, V_{bi} the built-in potential and, finally, M is the grading coefficient [27]. Schottky diode C_j is typically lower than a pn-junction diode, due to the lower physical dimensions of a metal-semiconductor junction.

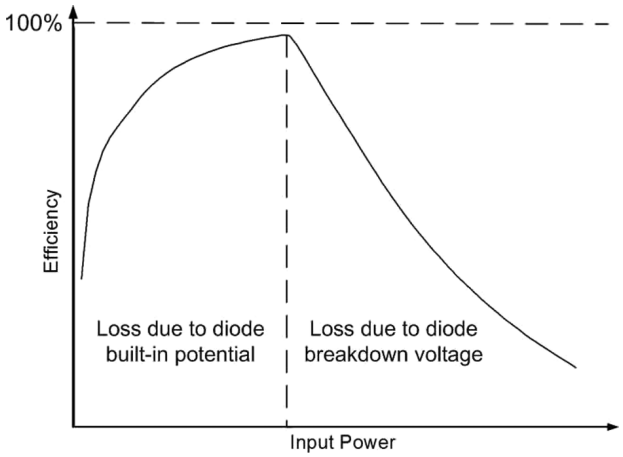

Figure 3.4: Conversion efficiency curve at different input power.

The junction resistance, R_j, is function of the bias current (I_b), the saturation current and the thermal voltage ($V_T = \frac{nkT}{q}$) according to 3.3 [25], as follow:

$$R_j = \frac{V_T}{I_S + I_b} \tag{3.3}$$

The saturation current, in turn, is dependent in the Schottky barrier dimensions.

The series resistance R_S is the result of diverse contact resistances in the Schottky diode and it doesn't contribute to the rectification, producing considerable losses and reducing the conversion efficiency. In fact, the series resistance is usually considered as linear, due to the slightly change behaviour [28].

Therefore, assuming an ideal impedance matching network, the diode is the main source of losses within the rectifier. The parasitics of the diode play an important role in the efficiency. Also, the harmonic generated within the diode induces the degradation of the efficiency, because the incident power at the diode will be utilised to generate not only the DC, but also the harmonics.

Despite the previous sources of loss constitute an important role in the efficiency, the two typically main responsible for the efficiency curve represented in Figure 3.4 [27] are as follow:

- V_{bi} – limits the efficiency in the low input power region. A minimum input power is required to overcome the potential barrier and, thus, rectification process occurs.
- B_V – limits the efficiency in the high input power region. When the input power is high, the reverse voltage across the diode overcomes the B_V and the efficiency decreases, although the output DC power remains constant.

A more accurate study regarding the Schottky diode characteristics is presented in Section 3.3, where their effect into the rectifier conversion efficiency will be evaluated through simulations.

3.2 Rectifier Topologies

A rectifier circuit can have many designations according to the position and number of non-linear elements. This section aims to discuss some of the different topologies that have been employed for RF-to-DC conversion. The half-wave rectifiers conducts half of the cycles, the positive or the negative cycles. On the other hand, a full-wave rectifier is able to conduct on both half-wave cycles of the input signal. However, at low incident power levels the full-wave rectifier is not efficient [29] and simple rectifiers, such as single-series or single-shunt diode configurations, are a better choice to obtain higher efficiency [3].

According to this briefly introduction and taking into account the goals for this work, are analysed three rectifiers: the single-series diode, the single-shunt diode and the voltage multiplier.

3.2.1 Single-series Diode Rectifier

The single-series diode topology, or envelope detector, is a well known half-wave rectifier widely adopted [23]. It is one of the most simple and cheaper rectifier solutions. Figure 3.5 presents this rectifier, where the series diode is the key element. There are also a filter capacitor and a load.

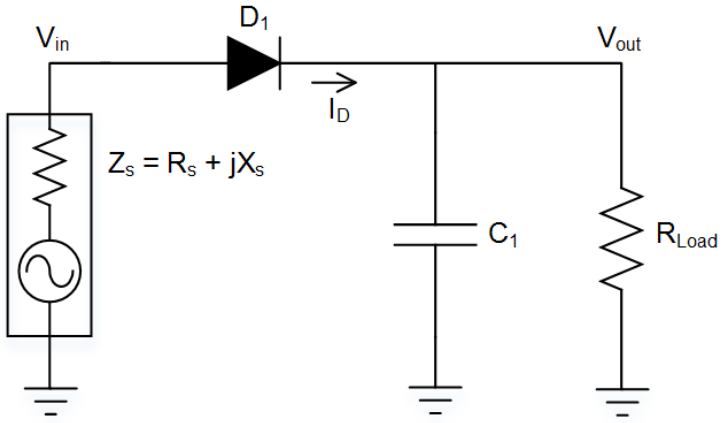

Figure 3.5: Single-series diode rectifier.

According to Figure 3.5, when the diode is forward biased, the current flows through it and charges the capacitor C, increasing V_{out} to the peak value (ideally equal to the input signal peak). Between successive peaks of the input RF signal the diode will be mainly reverse biased and, therefore, there is ideally no current flowing on the diode. The capacitor discharges through the load R and cause the V_{out} decrease relatively to its peak until the diode become forward biased. This effect is known as ripple. The time domain analysis of input and output voltages and current through the diode were simulated and plotted in Figure 3.6 for a certain time-scale, considering an ideal diode and sine wave as input signal in order to understand the rectifier behaviour.

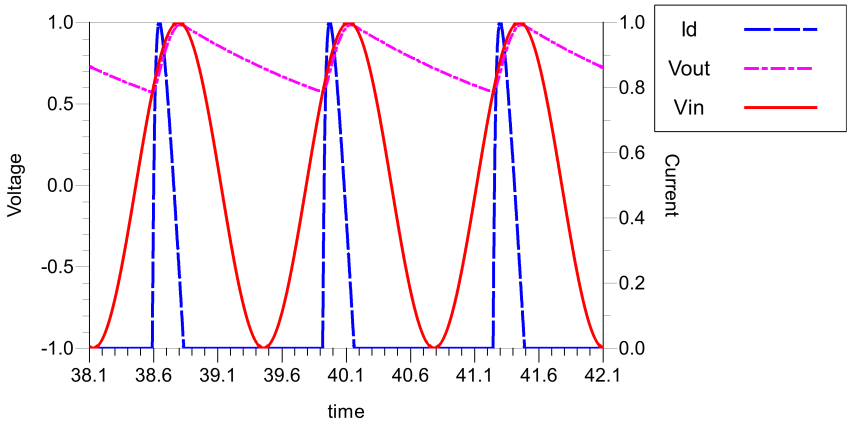

Figure 3.6: Single-series rectifier voltage and current curves.

The capacitor, besides provide a RF path to ground, also has to hold the output voltage level when the diode is reverse biased and then reduce the output ripple. Therefore, increasing the time constant τ (Equation 3.4)to values many times higher than the RF signal period T (Equation 3.5) is possible to keep the output voltage almost constant during period T. In sum, the capacitor C and resistor R should follow the relation in Equation 3.6.

$$\tau = RC \tag{3.4}$$

$$T = \frac{1}{f_{RF}} \tag{3.5}$$

$$RC \gg \frac{1}{f_{RF}} \tag{3.6}$$

3.2.2 Single-shunt Diode Rectifier

The single-shunt diode configuration, represented in Figure 3.7, is another simple rectifier. An input capacitor, a shunt diode, an RF inductor and a load constitute this topology.

Considering again an ideal diode with a sine wave excitation, as soon the diode becomes forward biased, the voltage V_d is clamped to 0 V and capacitor C is charged. In the reverse diode situation, V_d waveform is imposed by the input signal V_{In} added with a DC component introduced by the capacitor C. Since the charge in the capacitor remains almost constant, the DC component is roughly equal to the amplitude of the input signal V_{in}. Therefore, the lower excursion of V_d is ideally 0 V and the upper is two times V_{in} amplitude. Finally, the inductor L act as a RF choke preventing the RF to reach the load without constrain DC passage. In Figure 3.8 are presented the referred voltages, as well the current flowing through the diode during a certain time-scale.

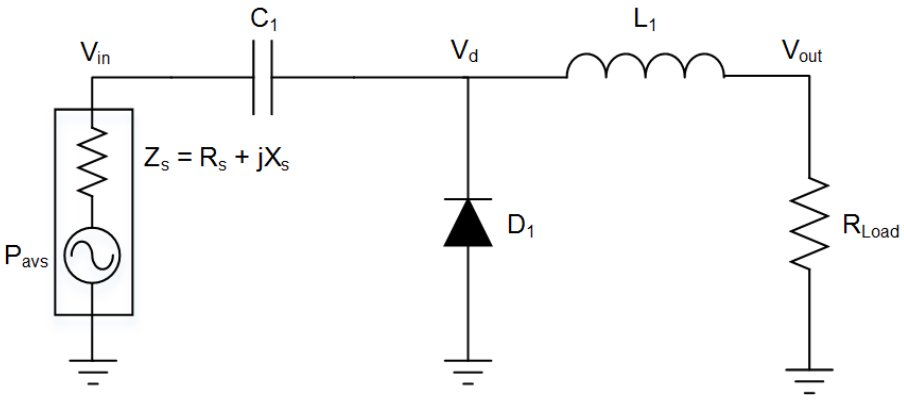

Figure 3.7: Single-shunt diode rectifier.

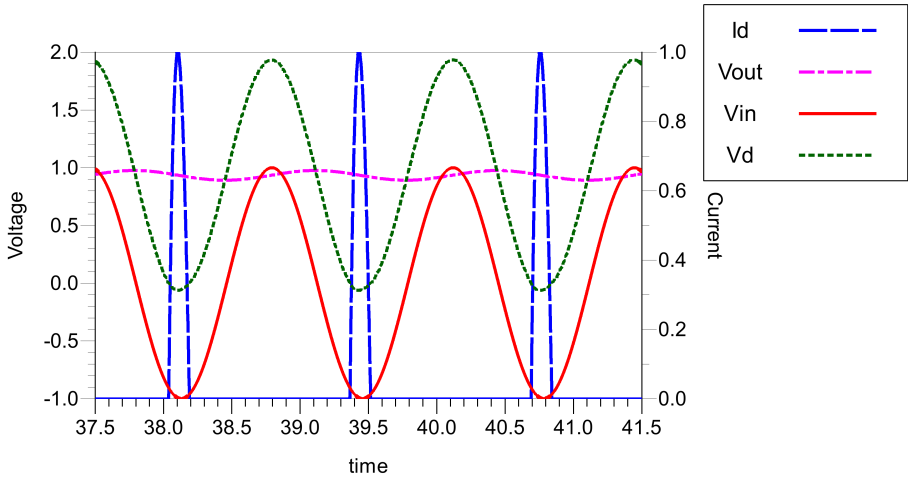

Figure 3.8: Single-shunt rectifier voltage and current curves.

3.2.3 Voltage Multiplier

Both single-series and single-shunt diode rectifiers can't afford an output voltage higher than the peak of the input RF signal. In turn, another half-wave rectifier solution is the voltage multiplier. Besides the rectification, it allows the voltage multiplication. This basic voltage doubler configuration, presented on Figure 3.9, is formed with two diodes, two capacitors and load. Basically, the voltage doubler is an envelope detector as shown in 3.2.1 with a DC level at its input.

Once again, assuming the same ideal conditions as previously, $D1$ is forward biased during the negative excursion of the input signal. Thus, the current flows through $D1$ and charges the input capacitor $C1$ to the most negative peak of the input signal (V_p). While $D1$ is forward biased, $D2$ is reverse biased than C1 keeps its charge. Thus, the capacitor $C1$ acts as a voltage source. On the other hand, the input positive signal excursion forces

$D2$ to be forward biased and $D1$ reverse biased. Therefore, capacitor $C2$ will be charged through $D2$. However, the DC level imposed by $C1$ added with the input signal forces $C2$ to be charged to double the peak of the input signal ($V_{out} = 2 \times V_p$). Of course, with the real diode the DC output voltage will be reduced by the threshold voltage on each diode. Figure 3.10 proves the higher output voltage level of the voltage doubler rectifier relative to the previously shown topologies.

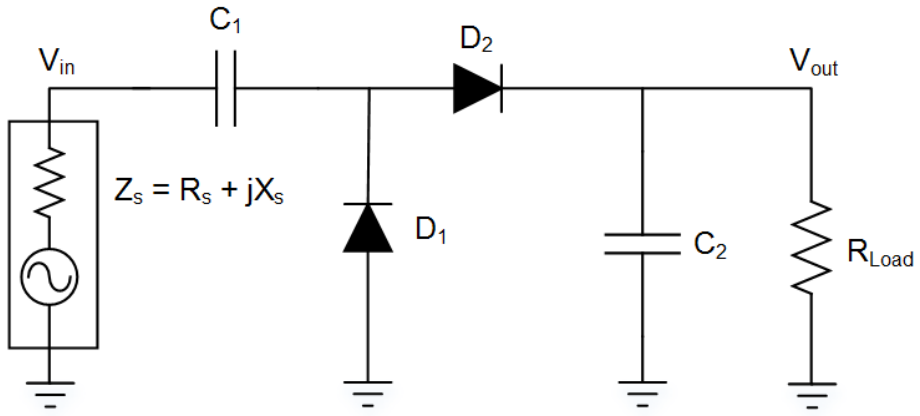

Figure 3.9: Voltage doubler rectifier.

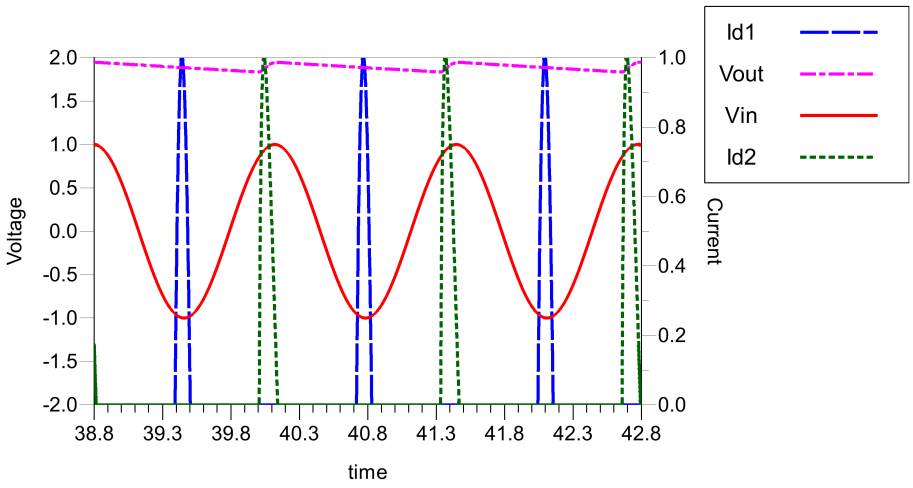

Figure 3.10: Doubler voltage and current curves.

The voltage doubler concept can be extended to a voltage multiplier by cascading the former. An example of a n-stage multiplier circuit is shown in Figure 3.11. The DC voltage provided for each stage acts as reference for the following stage. Hence, a voltage multiplier

can produce, theoretically, an output DC voltage as expressed in Equation 3.7.

$$V_{out} = 2n \times V_p \tag{3.7}$$

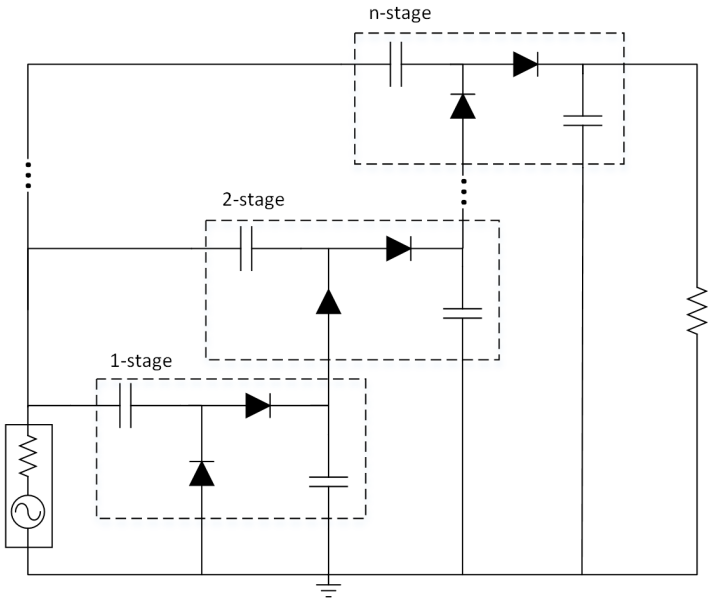

Figure 3.11: n-stage voltage multiplier.

Despite the increased output voltage, it should be noticed that as the number of stages increases, more components and line connections between them are required and then more power will be consumed. As result, will be obtained a lower rectifier conversion efficiency.

3.3 Simulation Survey

This section aims to complement the previous theoretical analysis through simulations. First, the diode non-linearities are study according to its effect in a rectifier conversion efficiency. Some commercial Schottky diodes performance is also simulated and compared with the non-linearities study. Finally, the topologies previously exposed are simulated with a real diode model in order to compare each other performance and to the expected to obtain with the theoretical approach. The simulation survey is made through ADS software.

3.3.1 Diode Non-linearities

In order to understand the diode efficiency response, its non-linearities are carefully studied. Thus, a Schottky diode as non-linear element in the single-series diode rectifier, as presented in Section 3.2, is the method followed for the referred study.

According to the State of the Art, provided in Section 2.4, the zero bias Schottky diode HSMS-2850 is widely employed for low input power. Therefore, the survey aims to evaluate the rectifier efficiency changes by changing the HSMS-2850 spice parameters around its nominal values, shown in Figure 3.12 [25]. The study is made without an impedance matching network between power source and rectifier and, thus, the efficiency performance along this survey is underestimate. Moreover, a similar study can be observer in [30].

SPICE Parameters

Parameter	Units	HSMS-285x
B_V	V	3.8
C_{J0}	pF	0.18
E_G	eV	0.69
I_{BV}	A	3 E-4
I_S	A	3 E-6
N		1.06
R_S	Ω	25
P_B (V_J)	V	0.35
P_T (XTI)		2
M		0.5

Figure 3.12: HSMS-2850 spice parameters.

Figure 3.13 presents the series diode rectifier efficiency versus the input power at 754 MHz for the junction capacitance, breakdown voltage, series resistance and saturation current variations around their nominal values. For each parameter variation, the remaining parameters are maintained with their nominal values.

According to Equation 3.2, the junction capacitance, C_j, is proportional to C_{j0}. Thus, the later is changed from its nominal value ($0.18pF$) to 2 and $4pF$. As shown in Figure 3.13a, the increase of C_{j0} (and consequently C_j) generates an efficiency reduction, more pronounced at lower input power levels. However and despite not presented in Figure 3.13a, it was verified that reducing C_{j0} to below the nominal not increase efficiency.

Regarding the breakdown voltage, B_V, it turns out that the lower it is, the lower is the range power of operation, circumscribing the efficiency to lower input power levels, as exhibited in Figure 3.13c. Therefore, to enhance the conversion efficiency over a wider range of input power levels, Schottky diodes with higher breakdown voltages are required.

Figure 3.13c shows the series resistance, R_S performance effect. As expected, R_S reduces the rectifier efficiency, due to the dissipation increase that occurs in the diode. Hence, the efficiency is improved to Schottky diodes with a low series resistance. Finally, as shown in Figure 3.13d, increasing the saturation current I_s is possible to obtain higher efficiency

levels, more perceptible for lower input power. Thus, is verified that saturation current affects the Schottky diode threshold voltage.

Another important analysis is the frequency response. In this case, among the previous non-linearities, junction capacitance is the only responsible for frequency deviations. Therefore, Figure 3.14 presents the rectifier efficiency over a frequency sweep from 0 to 5 GHz for three different C_{j0} values. As mentioned in the theoretical analysis, is verified that junction capacitance affects the high frequency response, acting as a LPF, especially for higher C_{j0} values.

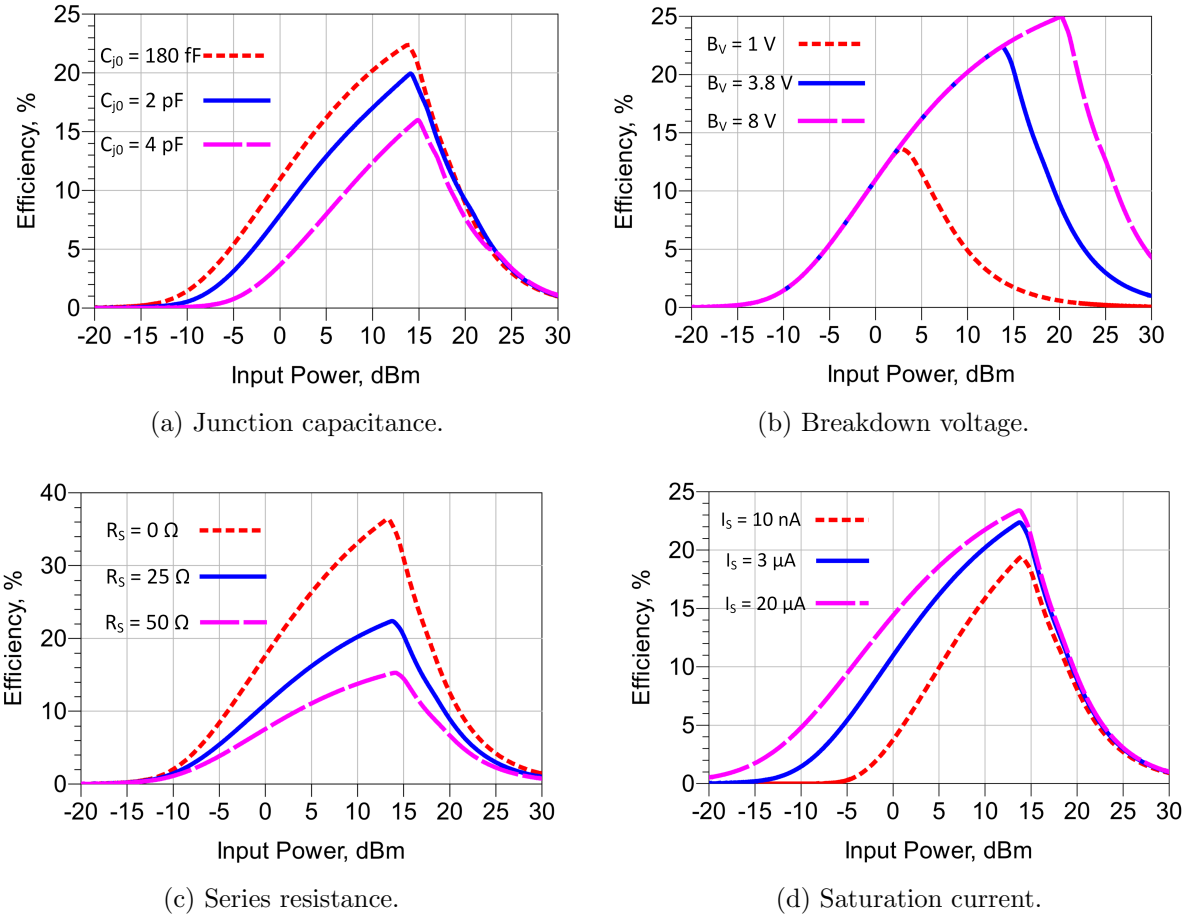

(a) Junction capacitance.

(b) Breakdown voltage.

(c) Series resistance.

(d) Saturation current.

Figure 3.13: Rectifier efficiency response versus input power for different parameters variations.

Despite each Schottky diode spice parameter was studied separately, it should be noticed that they are related to each other. Thus, the diode response is a compromise between all the non-linearities to obtain a desired performance, according to the frequency and the input power levels. For example, in practice, increasing B_V also implies an R_S increase. Thus, a Schottky diode design is a trade-off between high B_V and low R_S [28] and this explains their typically low B_V.

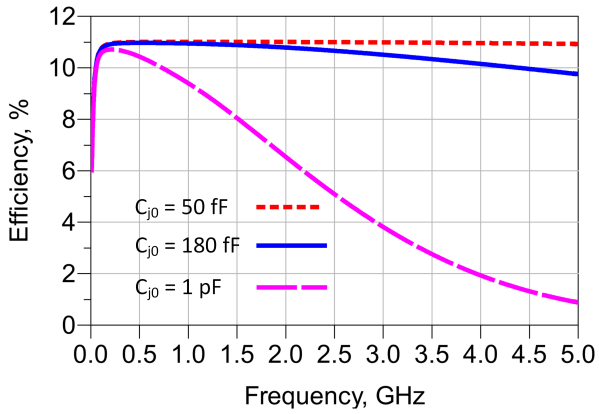

Figure 3.14: Rectifier efficiency response vs RF frequency for different C_j values.

3.3.2 Commercial Schottky Diodes

There are various commercial Schottky diodes. However, is important to evaluate their performance to make a reliable choice according to energy harvesting requirements. Therefore, a similar survey to the previous is carry out with different Schottky diodes, usually employed in EH systems. For each diode, it will be analysed and compared the response efficiency to an input power sweep between -20 to 30 dBm.

Into the four considered diodes, three are from Avago Techonologies (HSMS-2850 [25], HSMS-2820 [31], HSMS-2860 [32]) and one is from Skyworks (SMS7630) [33]. The results are shown in Figure 3.15 and is proved that both HSMS-2850 and SMS7630 have superior performance at low input power levels and improved sensitivity than the remaining Schottky diodes. Hence, it is justified the reason why both are widely employed for low power input levels, as shown in Section 2.4.

To understand these responses behaviour, are plotted in Figure 3.16 the IV-Curves for each diode. As expected, HSMS-2850 and SMS7630 start to conduct for lower forward voltages and hence, for lower input power levels. This explains their improved efficiency at lower input levels. Also, another conclusion to take from Figures 3.15 and 3.16 is that HSMS-2850 and SMS7630 have a lower junction voltage than HSMS-2820 and HSMS-2860 diodes, as can be verified in Table 3.1, where were summarized some spice parameters of the referred diodes.

Moreover, HSMS-2850 and SMS7630 have lower junction capacitances and higher saturation current (I_S) than HSMS-2820 and HSMS-2860. Therefore, according to the previous study, both this characteristics produces a significantly performance increase at low input power levels. The response at higher input power levels is then the limitation of HSMS-2850 and SMS7630, where HSMS-2820 and HSMS-2860 have a better performance. This behaviour can be justified by the breakdown voltage, which is higher for both HSMS-2820 and HSMS-2860 and, therefore, they reach the breakdown region at higher input power levels.

In sum, SMS7630 and HSMS-2850 are the more suitable for energy harvesting purpose.

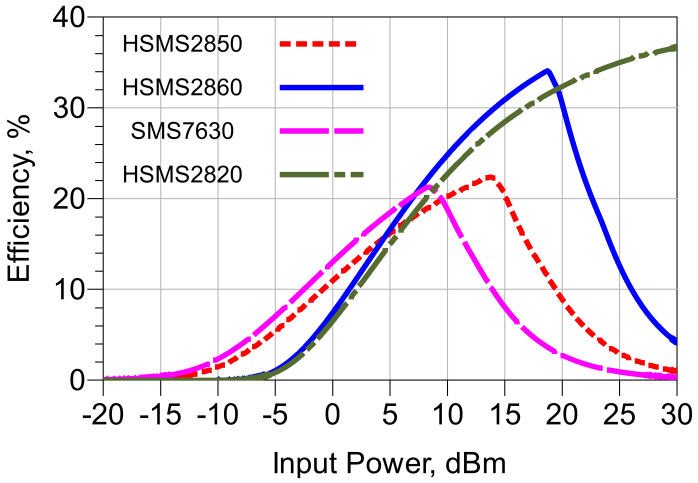

Figure 3.15: Rectifier conversion efficiency with different commercial Schottky diodes.

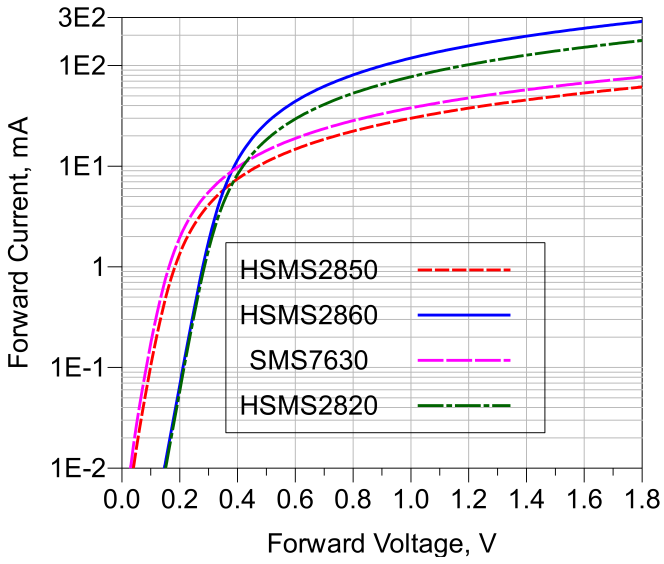

Figure 3.16: Commercial Schottky diodes IV-curves.

Furthermore, it should be noticed the slightly improved performance of the SMS7630 relative to the HSMS-2850.

As remaining note, the rectifier efficiency response is also related with other elements that weren't taken in concern, such as the impedance matching network, as previously mentioned, and load. Taking into consideration a proper matching network and load to each case, the efficiency deviations verified between each commercial diode should change, however, the same conclusions as before should be obtained. This note is also valid for the non-linearities survey.

	HSMS-2820	HSMS-2850	HSMS-2860	SMS7630
I_S	22 nA	3 μA	50 nA	5 μA
R_S	6 Ohm	25 Ohm	6 Ohm	20 Ohm
C_{J0}	0.7 pF	0.18 pF	0.18 pF	0.14 pF
B_V	15 V	3.8 V	7 V	2 V
V_J	0.65 V	0.35 V	0.65 V	0.34 V

Table 3.1: Commercial diodes spice parameters.

3.3.3 Rectifier Topologies

In this section, a simulation survey into the rectifiers topologies introduced in Section 3.2 is made to understand and validate the theoretical concepts. Besides the single-series and single-shunt topologies, there are shown three voltages multipliers simulation results – 1, 2 and 3 stages.

In the simulations it was considered the same Schottky diode model for all the rectifiers. The SMS7630 is the one adopted, due to its improved performance according to the previous study. In this case, the input reflection coefficient can significantly change between each configuration. Thus, promoting the adaptation between source and rectifier is important to take more reliable conclusions at the low input power levels. Due to the well operating point introduced by the matching network, it is optimized to -10 dBm.

According to Figure 3.17, efficiency at low input power is higher for the single-shunt rectifier. However, both single-series and the voltage doubler (1-stage multiplier) present appreciable efficiency at this input powers. On the other hand, the 2 and 3-stages voltage multipliers exhibit an improved performance at higher input power levels. This is justified by the increase number of diodes, that allow the respective configuration to handle more power.

Considering only the 1, 2 and 3-stages multipliers, besides the efficiency increase at higher input power levels its maximum tends to decrease with the increment of the number of stages.

Regarding the output DC voltage, the single-series diode configuration presents the lower maximum V_{DC}, followed by the shunt configuration and the multipliers, as depicted in Figure 3.18. Voltages multipliers with more than three stages will induce a higher maximum V_{DC}. At lower input power levels, it's not clear the differences between the configurations.

As final remark, the input power that leads to the maximum conversion efficiency in each rectifier is roughly the same that leads to the maximum V_{DC}. However, while efficiency decreases after its maximum, output voltage remains stable, as expected.

In sum, besides the single-shunt and series rectifiers, 1-stage multiplier also presents a considerable efficiency at low input power levels, as well higher output voltage. Therefore,

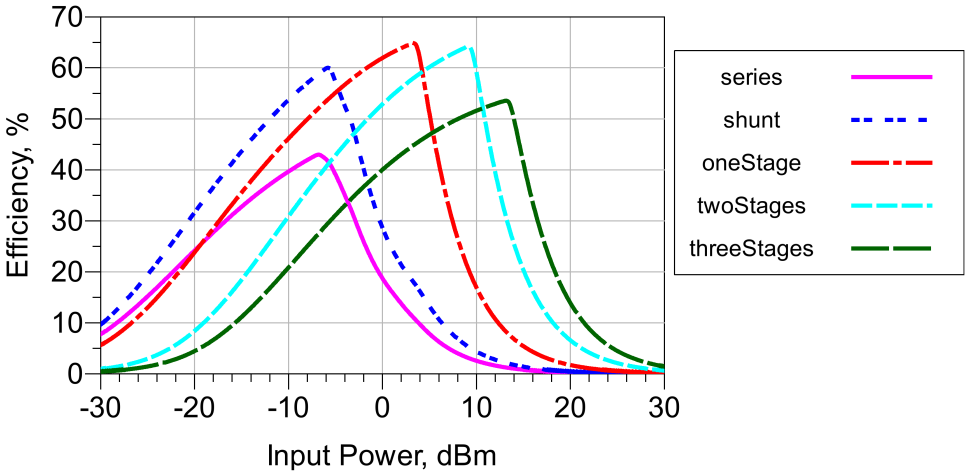

Figure 3.17: Efficiency versus input power for different configurations.

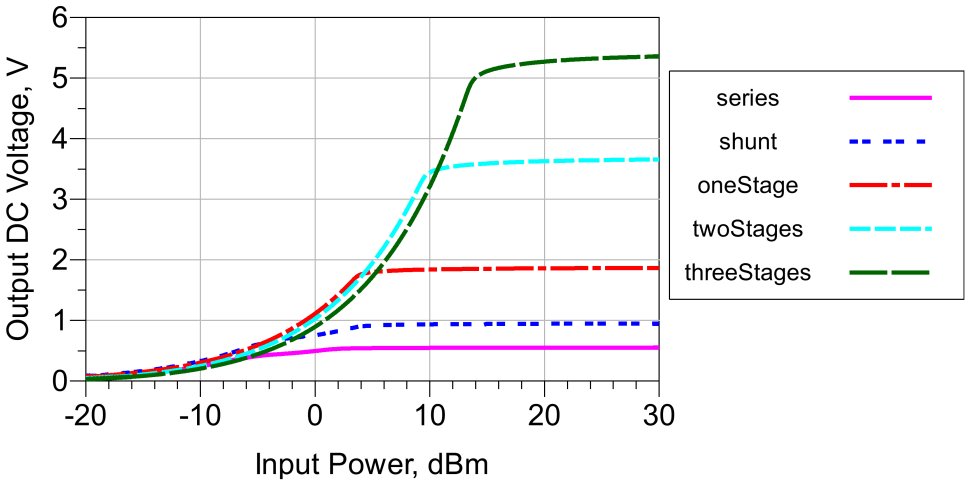

Figure 3.18: Output dc voltage versus input power for different configurations.

these configurations are suitable for EH, with emphasis in the single-shunt diode.

Chapter 4

Rectifier Circuit – Design and Measurements

This chapter focuses on the design proceedings and results of the rectifier stage. To achieve a high efficiency rectifier at low input power, is required an assertive decision upon the topology, the Schottky diode and load. Also, should be minimized the signal reflections, mainly with a proper matching network inclusion.

Therefore, attending to the project objectives and the analysis provided in Chapter 3, it will be presented the proposed circuits to proceed for the design and the Schottky diode. Then, some simulation steps until the final circuits are exhibited, including the load choice and the matching network design.

Moreover, the measurements proceedings are presented, as well the obtained results. This results are analysed and compared to the expected by simulation. Once again, the simulations are performed with ADS software.

4.1 Simulation Proceedings and Design

Before go forward with the rectifier design itself, is necessary to provide certain important considerations taken. First, it is intended to ensure a considerable performance for at least 200 meters away from the Aveiro central transmitter. In this range there is many potential EH system users. As analysed in Section 2.3, according to the Friis transmission formula (Equation 2.2), at 200 meters from the Aveiro transmitter is expected roughly -10 dBm. Closer to the transmitter and hence for higher input power, the system will not operate at its optimum efficiency, however, it doesn't mean, necessarily, a worse performance. Thus, along the design, the goal is to obtain the maximum possible conversion efficiency at -10 dBm, over all the D-TV channel.

As second and finally consideration, the dielectric substrate used for the rectifier is the Roger 5880 with $\epsilon_r = 2.2$ and 0.8 mm thickness. Despite the low ϵ_r, that increases the radiation, the choice is justified by the low tangent loss (0.0009) [34].

4.2 Proposed Circuits

According to the analysis provided in Section 3.3 and as already mentioned, the single-shunt, single-series and voltage doubler present improved performance at low input power levels, which is highly desired for EH. Thus, the three referred rectifiers are designed.

For both single-shunt and single-series diode rectifiers is adopted the SMS7630 Schottky diode, due to its slightly higher efficiency compared to the HSMS-2850, as proved in Figure 3.15. Despite this higher performance of the SMS7630, for the voltage doubler the choice was the HSMS-2852, that is a package with two HSMS-2850 diodes in series. Thus, the mounting process is simplified and the losses and extra parasitics of having two different packages that requires line connections between them are reduced.

The single-shunt rectifier design circuit is presented in Figure 4.1. Although the introduction of the RF choke in this configuration inhibits, theoretically, any RF signal to reach the load, excluding the need for an output capacitor, it was verified the presence of ripple in the output voltage. In order to minimize it was introduced an output capacitor (CL), as shown in Figure 4.1.

Regarding the single-series rectifier simulation schematic, presented in Figure 4.2, it was verified that the inclusion of an inductor to make the DC path to ground from diode anode to the load enhances the conversion efficiency. Of course, to prevent the RF to flow through the inductor, this needs to act as an RF choke. Hence, the commercial RF choke used in the single-shunt diode configuration also fulfils the requirements of the single-series.

Finally, the voltage doubler design circuit is shown in Figure 4.2, that is exactly as the presented in Section 3.2, besides the inclusion of transmission line and tee junctions required for the connections between the elements. The design of each proposed rectifier proceeds by choosing the proper load and design the matching network to enhance their performances.

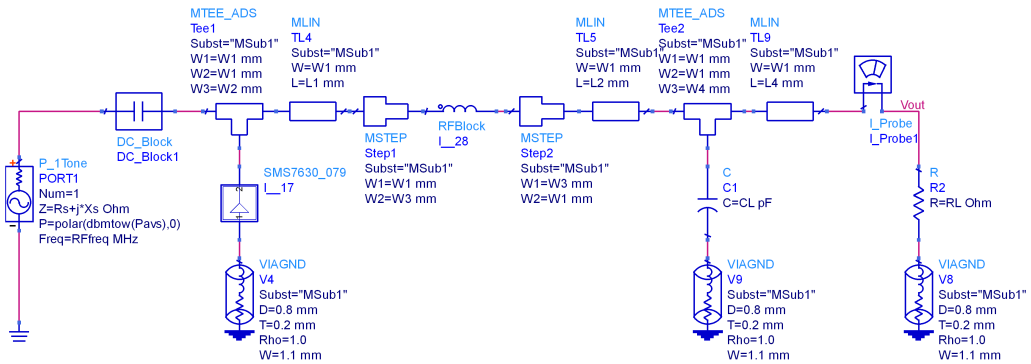

Figure 4.1: Single-shunt diode schematic.

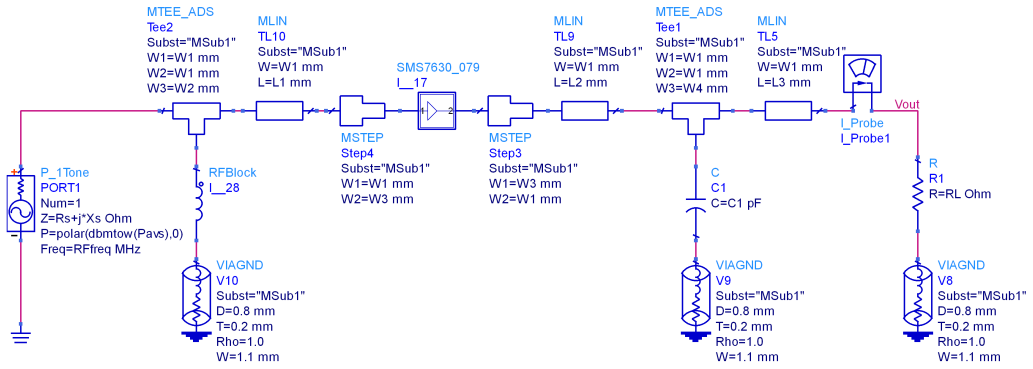

Figure 4.2: Single-series diode schematic.

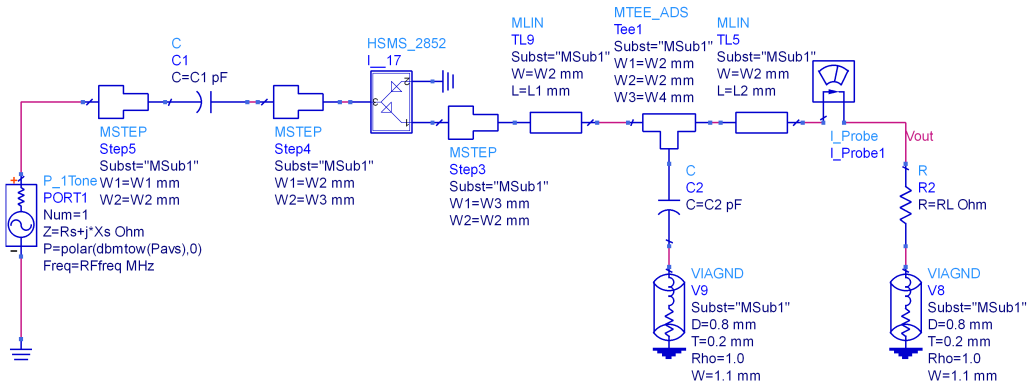

Figure 4.3: Voltage doubler schematic.

4.2.1 Load Choice

Figure 4.4 presents the maximum efficiency that is expected to obtain with different load R_L values for the -10 dBm input power at the central frequency of operation. This maximum efficiency is obtained through source pull simulations. Therefore, the efficiency at Figure 4.4 for each R_L is obtained with the respective input impedance that leads to the maximum efficiency.

The maximum efficiency for the single-shunt and single-series diode configurations is 68.4% with a load around 7000 Ohms and 71.6% with a load around 6200 Ohm, respectively.

However, these high load values require a most accurate source impedance and a good agreement between simulations and measures, because of the impedance sensitivity, where small deviations in the source impedance around the ideal produce a high decrease in the efficiency. For both cases, with a lower load the decrease is less significant. This is represented in Figure 4.5 for the single-shunt diode rectifier case. The efficiency profit obtained with simulations for the higher load can rapidly become an efficiency lack in practice. As consequence, a lower load is adopted to reduce the efficiency decrease with an eventually misalignment. Hence, the load is set to 3300 Ohm for the single-shunt

configuration and 3900 Ohm for the single-series.

For the voltage doubler configuration the analysis is similar. The efficiency takes a maximum at much higher loads, that is not represented in Figure 4.4 (around 30k Ohm). However, the problem of the high matching precision requirements for these higher loads was also verified. Therefore, the voltage doubler load is set to $7500Ohm$.

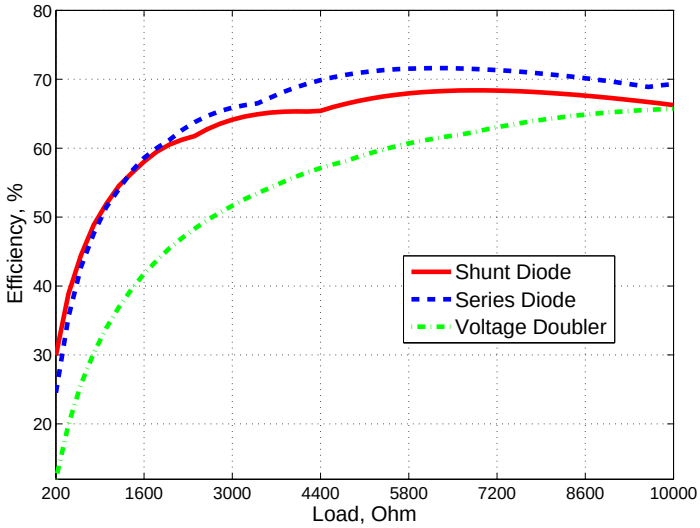

Figure 4.4: Efficiency versus load at -10 dBm input power.

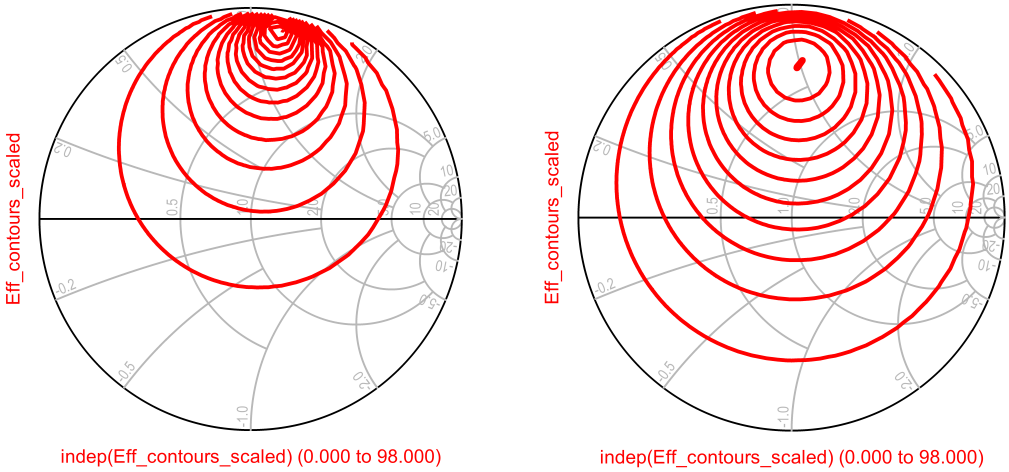

(a) $R_L = 7000Ohm$. (b) $R_L = 1000Ohm$.

Figure 4.5: Efficiency contours for the single-shunt diode configuration normalized to 250 Ohms.

4.2.2 Matching Network

The proper matching network between antenna (or power source) and rectifier is crucial to obtain an improved performance, as result of to the reflections minimization. The impedance to present to the rectifier is obtained, once again, through source pull simulations.

Thus, to each proposed circuit, with the respective load defined previously, the source pull indicates the impedance to present to the input of the rectifier that leads to the maximum efficiency. This impedance corresponds to the complex conjugate of the input impedance. As previously, the source pull simulation is set for the input power of -10 dBm and the central operation frequency. Thus, Table 4.1 shows the impedance Z_{In}^{*} – the complex conjugate of Z_{In} – to present to the each rectifier and the respective conversion efficiency that is expected to obtain for each rectifier at 754 MHz.

	Z_{In}^{*} (Ohm)	η_o (%)
Single-shunt	$26.0 + j234.3$	65.1
Single-series	$43.5 + j296.3$	66.6
Voltage doubler	$57.6 + j285.2$	63.9

Table 4.1: Source impedance for maximum efficiency to each configuration at 754 MHz.

According to Table 4.1, the efficiency is quite similar for the three rectifiers. Also, Z_{In}^{*} presents similar values to each other, as proved in Figure 4.6 with Smith Chart impedance locations.

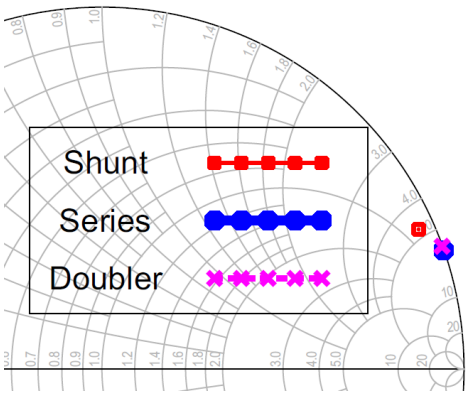

Figure 4.6: Smith chart representation of the source impedance for maximum efficiency at 754 MHz.

To avoid the lumped component parasitics is used a distributed matching network, despite the extra size imposed due to the high wavelength. There are several matching configurations that could be applied and some of them were considered in the simulations.

However, an open stub (with impedance Z_2 and length l_2) and a line (with impedance Z_1 and length l_1) was the adopted, as exemplified in Figure 4.7. This simple solution was preferable due to its small dimensions and adaptation effectiveness at the central frequency. Thus, the matching section must transform the source impedance Z_S to the impedance Z_{In}^*.

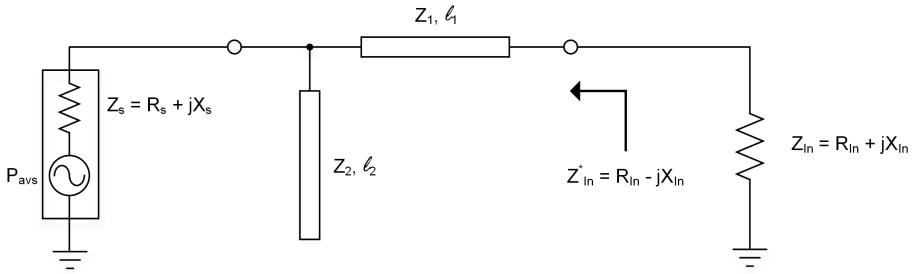

Figure 4.7: Distributed matching network.

As the impedances to present to each circuit are close, the procedures to design their matching networks are quite similar. Thus, the remaining matching network design steps and results are following summarized only for one configuration – the single-shunt diode rectifier.

Hence, the Smith Chart tool from ADS is used as first approach to project the matching network, as depicted in Figure 4.8. With this tool is provided the lengths required for the stub and line, maintained as first approach their impedance at 50 Ohms.

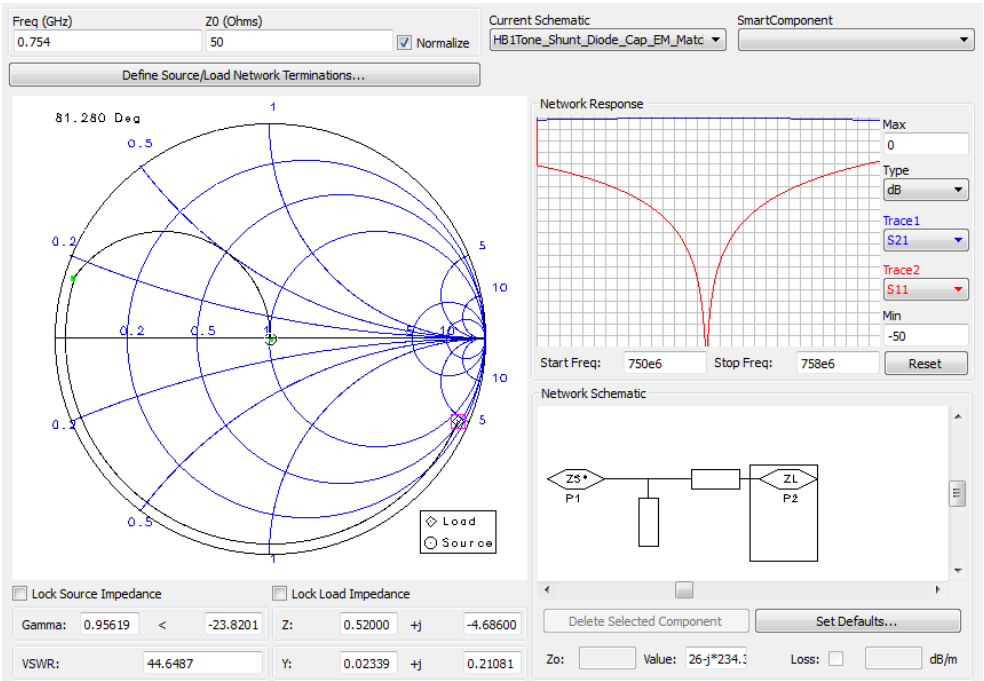

Figure 4.8: Smith Chart tool.

It worth notice that the matching produces losses and acts as a band-pass filter, reducing the bandwidth. To improve the bandwidth it would be required a more complex matching network. However, this increases the losses. In order to improve the matching network performance within all the operating band without increasing the complexity, it is made an optimization in the line and stub lengths and widths. Figure 4.9 shows the output return loss (S_{22}) relative to the input impedance and the forward gain (S_{21}) of the matching network, that proves the adaptation and verify the losses. This losses are verified in Figure 4.10, where the introduction of the matching network between the source and the rectifier produce a drop around 8.6% relative to an lossless matching network – the 67.1% efficiency drops to 58.5% at the central frequency.

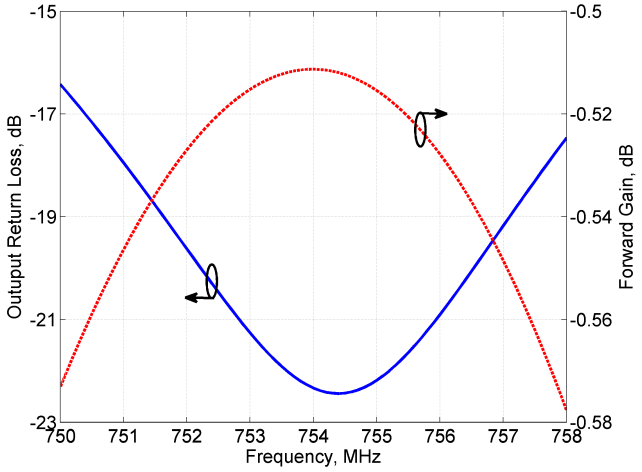

Figure 4.9: Output return loss and forward gain versus frequency of the shunt-diode matching network.

Moreover, the matching network achieved occupies a large portion of all the rectifier. To reduce the occupied area and, consequently, the cost, the matching network was comprised through the introduction of curves in the line and open stub. The layout of first matching network is presented in Figure 4.11a and the compression process has resulted in the layout shown in Figure 4.11b.

4.2.3 Electromagnetic Simulation

To increase the confidence and probabilities of the rectifiers success is required EM simulation. Momentum is a 3D planar electromagnetic simulator from ADS, that employs frequency-domain Method of Moments (MoM). This simulation allows an evaluation of the coupling between lines and parasitics, resulting in a more accurate simulation.

Therefore, after developing the layouts it was carried out EM simulation for the three rectifiers. The key parameters in the EM simulation are the mesh and frequency. The mesh is the set of cells that covers the entire circuit. As the number of meshes per wavelength

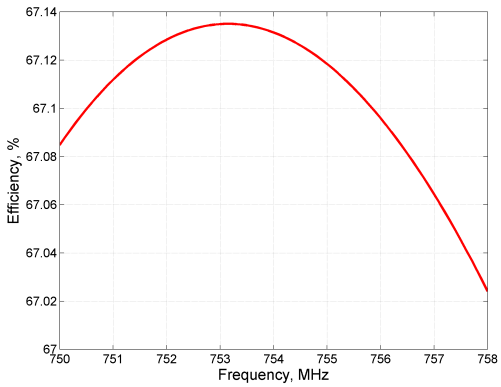

(a) With ideal matching network.

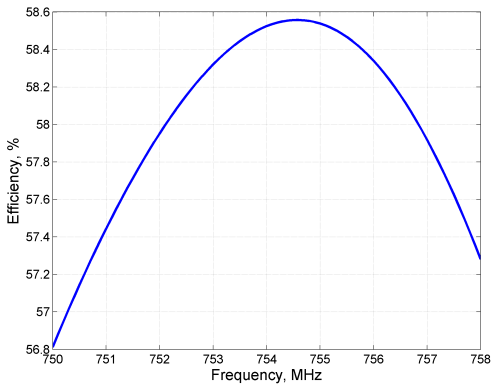

(b) With lossy matching network.

Figure 4.10: Single-shunt diode rectifier efficiency versus frequency.

(a) Before compression.

(b) After compression.

Figure 4.11: Matching network layout of the single-shunt diode rectifier.

increases, the simulation becomes more accurate, however more time-consuming. For the present work, the number of mesh cells was increased until changes in the S-parameters

relative to the previous simulation (with less mesh cells) weren't verified. Regarding the frequency, the EM simulation was performed for all the entire operating band and harmonics.

The EM simulation of each rectifier results in a slightly frequency deviation comparing to the circuit simulation. As consequence, small changes in the matching elements lengths were conducted to correct the mismatch. The single-shunt diode rectifier EM simulation is presented in Figure 4.12, where are visible the mesh cells. As remaining note, the pieces of cooper added closer to the matching network allow a manual tuning in case of deviations being verified in practice.

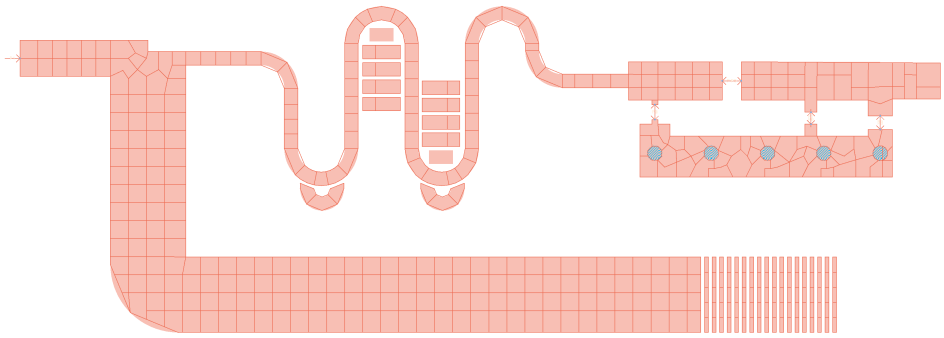

Figure 4.12: EM simulation for the single-shunt diode rectifier.

4.2.4 Prototype Rectifiers

After concluding the simulations, the circuits presented in Figure 4.13 were implemented. Despite already mentioned along the rectifiers design, Table 4.2 summarizes the components employed in each rectifier configuration. Additionally, it also presents their dimensions and becomes evident the similar length and width between each other.

	Single-shunt	Single-series	Voltage doubler
Dimensions	$32 \times 61mm$	$31 \times 59mm$	$32 \times 59mm$
Diode	SMS7630 (Skyworks)	SMS7630 (Skyworks)	HSMS-2852 (Avago)
RF Inductor	390 nH (Coilcraft)	390 nH (Coilcraft)	–
Load	3330 Ohm	3900 Ohm	7500 Ohm
Capacitor	100 pF	100 pF	100 pF [(1)]

[(1)] The same value for both capacitors.

Table 4.2: Summarized prototype rectifiers characteristics.

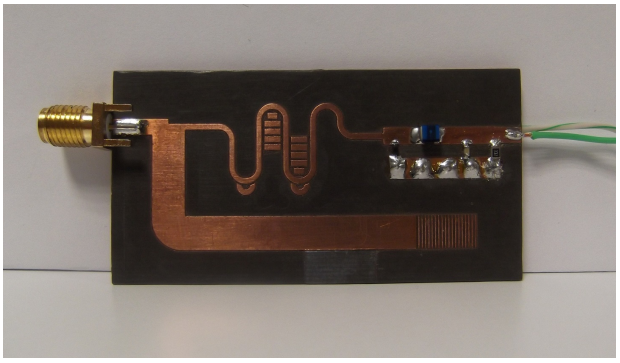

(a) Single-shunt diode.

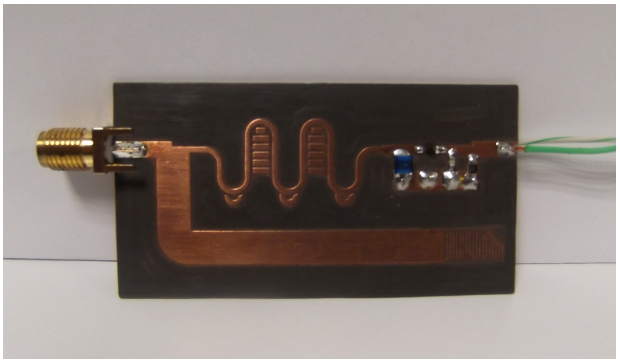

(b) Single-series diode.

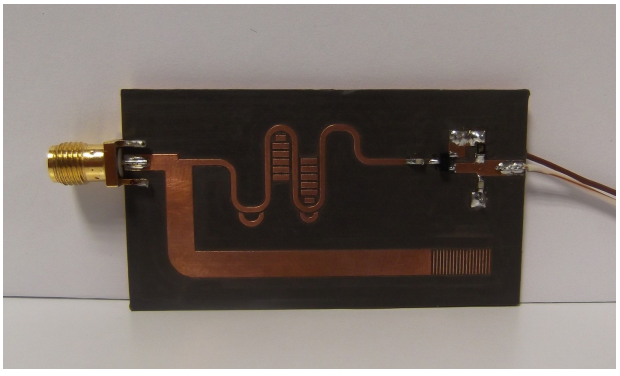

(c) Voltage doubler.

Figure 4.13: Prototype rectifiers.

4.3 Measurements Proceedings and Performance

To evaluate the performance of the rectifiers it is intended to measure the output DC voltage and the conversion efficiency to compare with the expected by simulation. The measurements were made using the following equipment:

- Signal generator – HP E4433B
- Spectrum analyser – R&S FSH13
- Programmable multimeter – HM 8112
- Network analyzer – Agilent Tech E8361C

To perform the output DC voltage and the efficiency, the rectifier circuit is excited through the Signal Generator (SG). The excitation signal is a single-tone with a certain power level. Nevertheless, the power was measured with the SA through the SMA cable that will also connect to the rectifiers and was verified a drop of the power level received due the cable losses. Therefore, to excite the rectifiers with a certain power level is necessary to set a slightly higher power level in the SG. Figure 4.14 presents the spectrum measure setup, where is evident the difference between the power level set in the generator and the actually power measured with the SA.

Next, the output DC voltage at the load of each rectifier is measured with the multimeter for a certain frequency and power level. The efficiency is then calculated using Equation 2.3. As small changes in the measured output DC voltage cause significantly deviations in the efficiency, the employed multimeter has high precision, resulting in a more accurate evaluation of the rectifier performance than a standard multimeter. Figure 4.15 presents the DC voltage measurement setup. The results are shown in Section 4.3.1.

(a) Spectrum measure setup.

(b) Spectrum analyser display.

Figure 4.14: Spectrum measure of a single-tone signal.

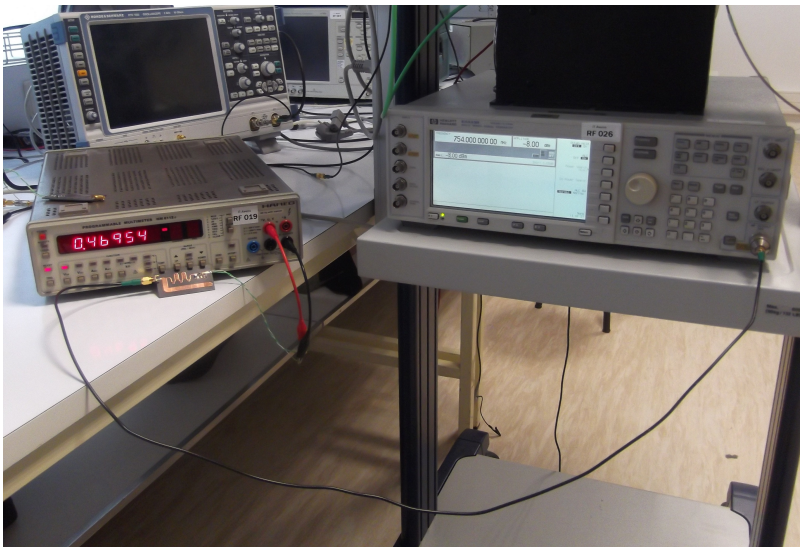

Figure 4.15: DC voltage measure.

4.3.1 Results

For each rectifier were carried out three measures. Firstly, with the input power set to -10 dBm, the frequency was swept between 730 and 770 MHz. Then, the reverse situation was performed – the frequency was set to 754 MHz and the input power was changed from -30 to 0 dBm. The output DC voltage and efficiency are plotted for both frequency and input power sweeps. Finally, the return loss $S_{11}(dB)$ was measured along the same frequency band. To evaluate the feasibility of the performed simulations, all the measures results are followed with the respective simulations results.

The performance of the single-shunt diode rectifier is presented in Figure 4.16. Regarding the single-series diode, the results are plotted in Figure 4.17 and finally, Figure 4.18 focuses on the voltage doubler performance.

4.3.2 Analysis

Regarding the single-shunt diode rectifier and focusing in the frequency response presented in Figure 4.16a, the maximum efficiency is 57.8% and occurs at the central frequency of the operating band. As expected, the output voltage has the same behaviour, being the maximum around 0.44 V. Figure 4.16b presents the efficiency response to the input power and it is notorious that both efficiency and output DC voltage increase with the input power. From -30 dBm to around -4.5 dBm measurements and simulations present a good agreement. However, while simulations indicate a maximum efficiency at -4.5 dBm followed by a rapidly decrease, measured efficiency keeps increasing and, although it's not clear, it seems that its maximum is reached at around 0 dBm. This behaviour is due some underestimation in the SMS7630 diode model used.

The single-series diode has a maximum efficiency of 53.8% and a maximum output

DC voltage of 0.46 V at the lowest edge of D-TV operating band (750 MHz), as shown in Figure 4.17a. Thus, this constitutes a deviation from the simulations, that has a maximum of 58% at 754 MHz. About the response to the input power presented in Figure 4.17b, the behaviour is similar to the single-shunt diode rectifier, as expected. This is explained by the same Schottky diode and their similar configurations and load value. Nevertheless, the difference between measured and simulated results are more clear than in the single-shunt diode.

About the voltage doubler rectifier, it presents 57.1% maximum efficiency and 0.65 V maximum output DC voltage at 754 MHz, as shown in Figure 4.18a. These maximums are near the expected by simulation (58.3% and 0.66 V at 756 MHz, respectively). As regards to the efficiency response relative to the input power, it is presented in Figure 4.18b and is verified a good agreement between measurements and simulations. In this case, for the same input power level, the correspondent DC output voltage is higher than the ones obtained with the single-shunt and series diodes rectifiers. Moreover, the model of the respective employed Schottky diode does not constrain the performance at the higher measured input power levels, in contrast to the previously analysed rectifiers.

The input reflection coefficient presents a deviation from the simulation results for all the rectifiers. The optimum point was shifted for a lower frequency than the expected. Single-shunt diode rectifier presents the lowest shift between simulations and measurements (4 MHz) and single-series diode exhibits the highest shift (10.7 MHz). This shift explains the reduced efficiency at higher frequencies and the improvements at the lowers ones verified in the three rectifiers comparing to the simulations results.

In sum, the expected performance through simulations are quite similar to the three rectifiers regarding the conversion efficiency frequency response. Single-shunt diode rectifier presents the best simulation versus measurements within the channel 56 D-TV band (750 MHz to 758 MHz). On the other hand, voltage doubler measurements expose the closest response performance to the input power and, despite efficiency for 0 dBm being similar to the other rectifiers, it has more output DC voltage. Moreover, voltage doubler maintain a better performance than single-shunt diode rectifier outside the D-TV frequency band.

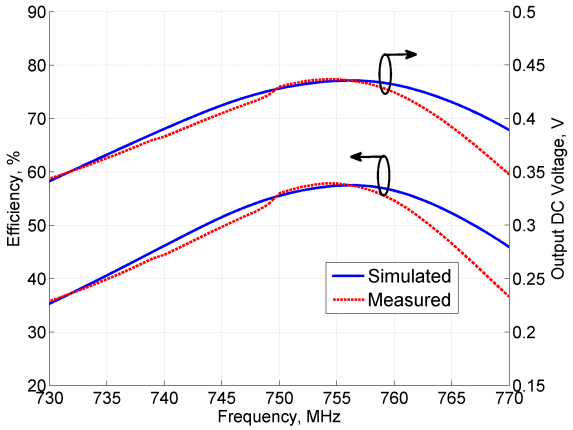

(a) Efficiency and output DC power versus frequency with $P_{avs} = -10dBm$.

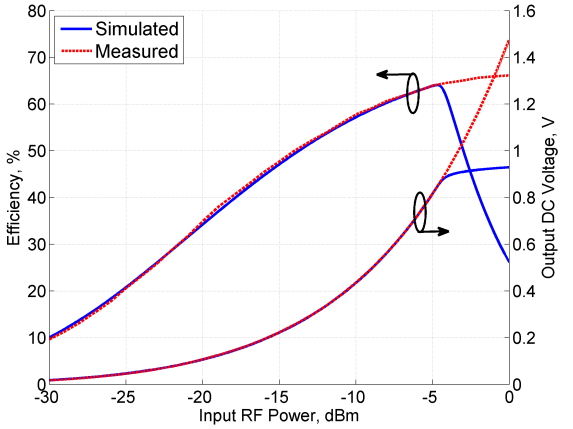

(b) Efficiency and output DC power versus input power with $Frequency = 754MHz$.

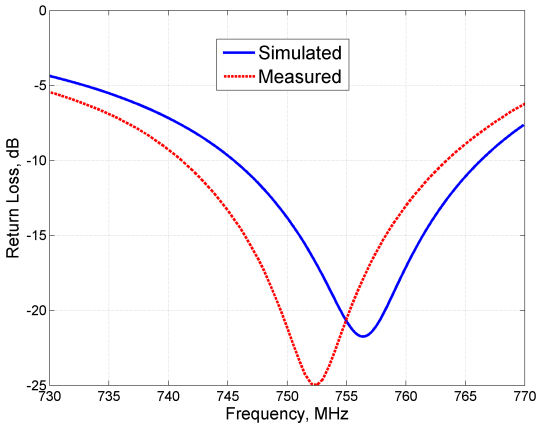

(c) Input reflection coefficient.

Figure 4.16: Simulated and measured results for single-shunt diode configuration.

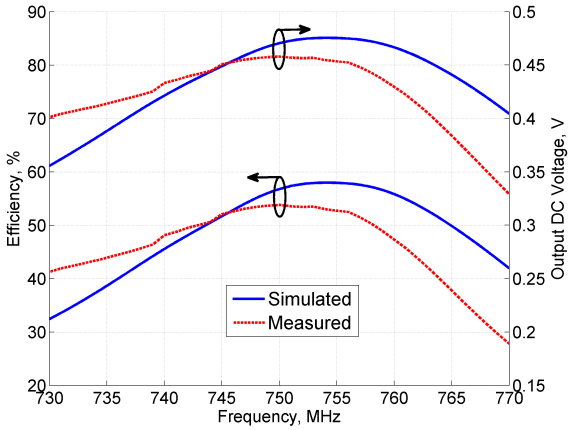

(a) Efficiency and output DC power versus frequency with $P_{avs} = -10dBm$.

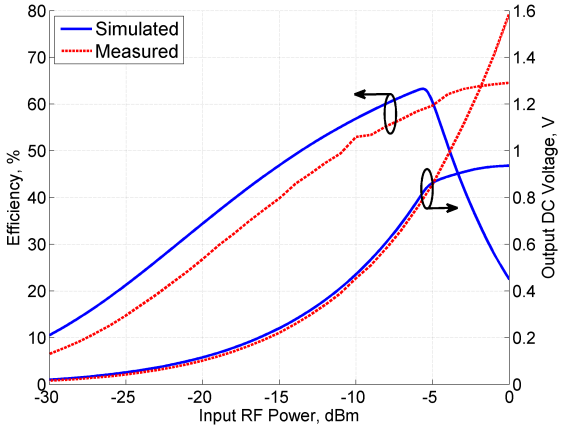

(b) Efficiency and output DC power versus input power with $Frequency = 754MHz$.

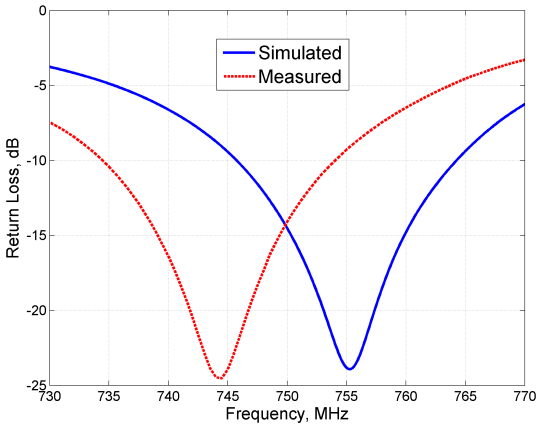

(c) Input reflection coefficient.

Figure 4.17: Simulated and measured results for single-series diode configuration.

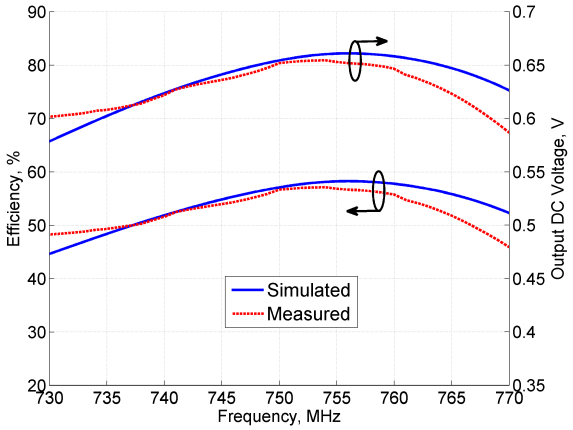

(a) Efficiency and output DC power versus frequency with $P_{avs} = -10dBm$.

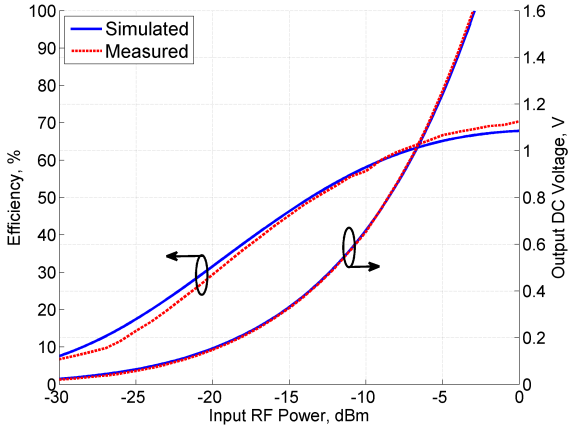

(b) Efficiency and output DC power versus input power with $Frequency = 754MHz$.

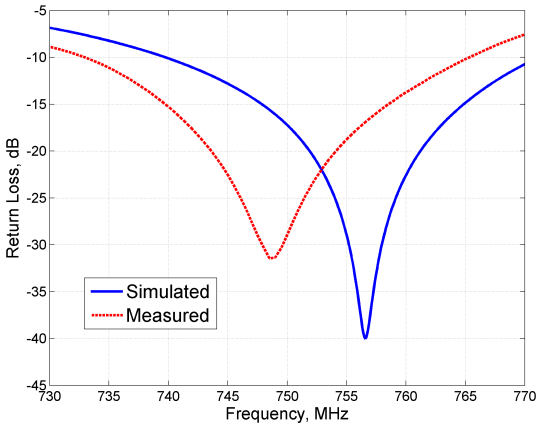

(c) Input reflection coefficient.

Figure 4.18: Simulated and measured results for voltage doubler configuration.

Chapter 5

Receiver Antenna

In this chapter is analysed and proposed the receiver antenna responsible to collect the electromagnetic energy in the environment. To obtain an EH system with improved performance, the receiver antenna should be able to collect the entire Portuguese D-TV 56 channel with a considerable gain able to provide a wide-reaching system. In addition, it is intended a low-cost antenna.

The chapter begins by introducing basic theoretical concepts that will be taken into account during the design and measurement processes. The fundamentals upon the microstrip patch antenna are also addressed, justifying its choice as starting point for the EH system receiver antenna. To improve the main microstrip patch limitation – the bandwidth – some solutions are suggested.

Regarding the antenna design, the steps followed through simulations are presented. Along with the simulation process, parametric studies also take an important focus in this section to improve the antenna performance and support the final antenna. Then, the proposed antenna is presented as well the respective simulation results.

To finalize the chapter, are presented the prototype antenna and the respective performance. This is compared with the expected to obtain through simulation.

5.1 Antenna Basics

The basic antenna characteristics presented in this section intend to cover the mainly concepts considered and analysed during the antenna simulations and measurements processes. A more detailed explanation about the following and other antenna characteristics can be found in [35].

5.1.1 Antenna Bandwidth

The bandwidth of an antenna defines the range of frequency over which the antenna characteristics are within an acceptable value and then is able to radiate or receive energy.

Bandwidth is usually expressed according to the input return loss or the equivalent VSWR. The minimum VSWR is 1 and dictates that 0% of the signal is reflected. A specific VSWR criterion may be employed to define antennas bandwidth.

To describe the bandwidth of narrowband antennas is often used the percentage of the frequency difference relative to the centre one,

$$BW\% = \frac{f_H - f_L}{f_c} \tag{5.1}$$

where f_H and f_L are, respectively, the highest and the lowest frequency in the band and f_c is the centre frequency.

In turn, broadband antennas bandwidth is described based only in the upper and lower acceptable operation frequencies, as expressed in Equation 5.2.

$$BW = \frac{f_H}{f_L} \tag{5.2}$$

5.1.2 Gain

Another important figure of merit in the antenna performance analysis is the gain. Unlike an ideal isotropic antenna, a real one will radiate more energy to some directions than to others. Therefore, gain is a measure related to the directivity. The gain of an antenna in a given direction is the ratio between the energy radiated and the energy that would be radiated if the antenna was hypothetically isotropic with the same input power.

As consequence, gain is usually expressed in dBi, i.e., the logarithmic gain (decibel) referenced to an isotropic antenna.

5.1.3 Polarization

The wave radiated or received by an antenna is characterized according to the electric-field (E) direction and establishes the antenna polarization.

In general, polarization can be classified as linear, circular or elliptical. The differences between the three polarizations are as follow:

- Linear polarization – electric-field vector is always directed along a line at every instant time and constitutes the simplest polarization form. Linear polarization can be divided into vertical or horizontal polarization depending if the electric-fields vector are perpendicular or parallel to the Earth's surface;
- Circular polarization – the electric-field direction changes, but its amplitude remains the same. Therefore, E appears to be rotating with circular motion along the propagation direction.
- Elliptical polarization – as the circular polarization, elliptical have two orthogonal electrical-field vectors, however with different amplitudes, describing an ellipse on the time domain.

A mismatch polarization occurs when transmitter and receiver antenna have different polarizations. The mismatch polarization loss can be estimated according to the Polarization Loss Factor (PLF), expressed in Equation 5.3,

$$PLF = |\cos \psi_P|^2 \tag{5.3}$$

where ψ_P is the misalignment between the antennas.

From Equation 5.3 is possible to verify that the PLF between two different linear polarization antennas (vertical and horizontal) is zero and, theoretically, communication between them isn't possible. A not so critical situation is the link between circular and linear polarization antennas. In this case, half the power will be loss, but it's possible to establish communication.

5.2 Microstrip Patch Antenna

Microstrip patch antennas are considered one of the most versatile antennas. They are also known for their low profile, inexpensive and fabrication simplicity. Furthermore, the easy resonant frequency and input impedance adaptability are other remaining reasons for their popularity.

As shown in Figure 5.1, the microstrip patch antenna is characterized by a conducting patch printed on a grounded dielectric substrate with permittivity ε_r and thickness h. The dielectric constant is considered the most sensitive parameter in the microstrip patch antenna [36]. Thus, an accurate characterization of the dielectric assumes an important role to the microstrip antenna design.

5.2.1 Rectangular Microstrip Patch

The microstrip patch antenna can assume diverse shapes, such as rectangular, circular. The well known equations associated with the advantages inherent to microstrip antennas stated before, make rectangular patch the most widely employed in a variety of applications.

The patch is described by the length L, width W and the feed point relative to the patch edge ($y0$), as exhibited in Figure 5.2, where was omitted the ground plane.

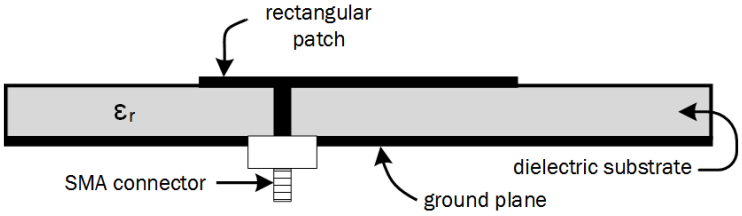

Figure 5.1: Microstrip patch antenna – side view.

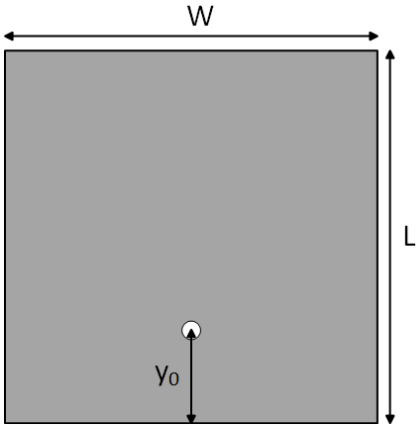

Figure 5.2: Basic microstrip patch antenna configuration.

To compute the patch dimensions W, L, equations 5.4 and 5.5 are used, where ε_{reff} is the effective dielectric constant and ΔL is the extension of the length. These and the remaining design equations can be found in [35].

$$W = \frac{c}{2f_r}\sqrt{\frac{2}{\varepsilon_r + 1}} \tag{5.4}$$

$$L = \frac{c}{2f_r\sqrt{\varepsilon_{reff}}} - 2\Delta L \tag{5.5}$$

5.2.2 Feeding Techniques

According to Equation 5.5, the patch length L is about half-wave length and then the current is lower at the patch edge and increases, in magnitude, towards the centre. As consequence, impedance take the maximum value at the edge of the patch and the minimum at its center. Therefore, a feed directly in the edge of the patch leads to high input impedance and many times is required to introduce the feed somewhere else within the patch. There are different methods to feed patch antennas. Two of the most popular schemes are the line feed and the probe feed, both contacting techniques.

The line feed scheme has the most easier fabrication process, because only requires one layer substrate and no hole. The microstrip line is placed in contact with the patch, as presented in Figure 5.3.

The probe feed technique is as shown in Figure 5.1. The coaxial outer is attached to the ground plane and the inner conductor is extended through the substrate and then connected to the patch. This configuration allows a easy matching, since the connector can be placed anywhere within the patch. Other advantages of this method are also the easy fabrication process and it has low spurious radiation. However, this method introduces an inductance that can lead to adaptation problems, especially for thick substrates.

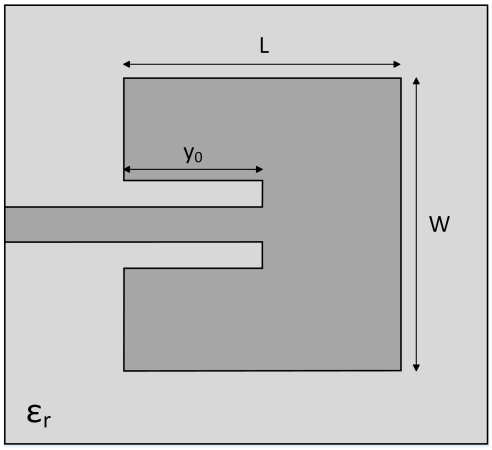

Figure 5.3: Line feed – top view.

There are two other main feed techniques that, being non-contacting, were introduced to overcome some of the contacting feed problems: the aperture-coupled and the proximity-coupled feeds [35].

5.2.3 Bandwidth Enhancement Techniques

Despite the previously mentioned qualities regarding the microstrip patch antenna, there is a main disadvantage – the narrow bandwidth. The typically bandwidth is between 3 and 6%, which is not adequate for some applications. In fact, the bandwidth constrain is principally due to the dielectric substrate permittivity, that assumes considerable values.

As attempt to overcome this problem, various solutions have been studied and used. Mainly, these solutions consist in changing the basic microstrip patch antenna structure. A good agreement between the basic antenna structure and the added elements has to be taken to reach the desired performance. Following are exposed some of the referred techniques.

Gap-coupled Parasitic Elements

The gap-coupled parasitic patches along the main feeding patch, as shown e.g. in [37], increases the microstrip patch antenna bandwidth. An example of this technique with two parasitic elements is presented in Figure 5.4.

The parasitic elements should be designed to resonate at around the same main patch resonance frequency, resulting in a bandwidth enhancement. Beyond the feeding and parasitics patches physical dimensions (width and length), also the gap between them play an important role to achieve the desired bandwidth behaviour.

This technique is easy to build, however a larger surface is required.

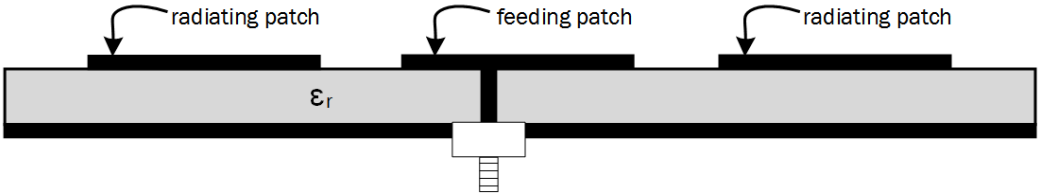

Figure 5.4: Gap-coupled parasitic patches configuration example.

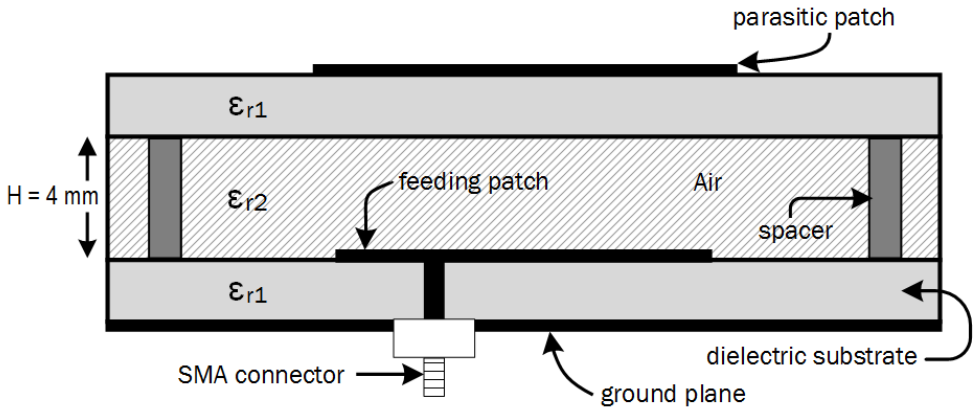

Figure 5.5: Stacked microstrip patch configuration example.

Stacked Microstrip Patch

Another bandwidth enhancement technique is the parasitic patches introduction above the main feeding patch, creating a stacked patch antenna. One possible configuration for a stacked antenna is presented in Figure 5.5.

The top patch, the parasitic, is placed in a second dielectric substrate without ground plane. The patches can be etched in equal dielectric substrates – same thickness and permittivity. However, great bandwidth improvements are reached when the bottom (feeding patch) has higher permittivity than the upper (parasitic patch) [38].

The feeding and parasitic patches are separated by an air gap space H highly dependent on wavelength and electrical characteristics of the used substrates. Instead of air gap, foam is also used as gap between the two patches, discarding the use of spacers. In order to fulfil the performance requirements, more than one parasitic element can be combined in the stacked patch antenna.

The air gap changes the coupling between the two elements and, therefore, the bandwidth [38]. It is the key in this technique. In the literature, thickness between around $0.05\lambda_0$ and $0.15\lambda_0$ are applied [38][39]. The patches physical lengths affects mainly the resonant frequency.

Slotted Microstrip Patch

The introduction of slots within the patch is often used to improve the bandwidth. The slot can assume many geometries. In literature are suggested, for example, U-slot[40][4], E-slot[4], C-slot [4] or rectangular [41] shapes onto the microstrip patch. In Figure 5.6 are presented the U-slot, the E-slot and the C-slot microstrip patch antennas proposed in [4].

Unlike the gap-coupled and staked elements techniques, the slotted patch generally doesn't requires extra surface area and it's still also able to induce new resonant frequencies. Again, combining the resonant frequencies of the patch with the ones caused by the slots is possible to increase the bandwidth.

According to the theoretical concepts present in [41], the slots change the patch inductance, which, when carefully designed, can significantly increase the antenna bandwidth.

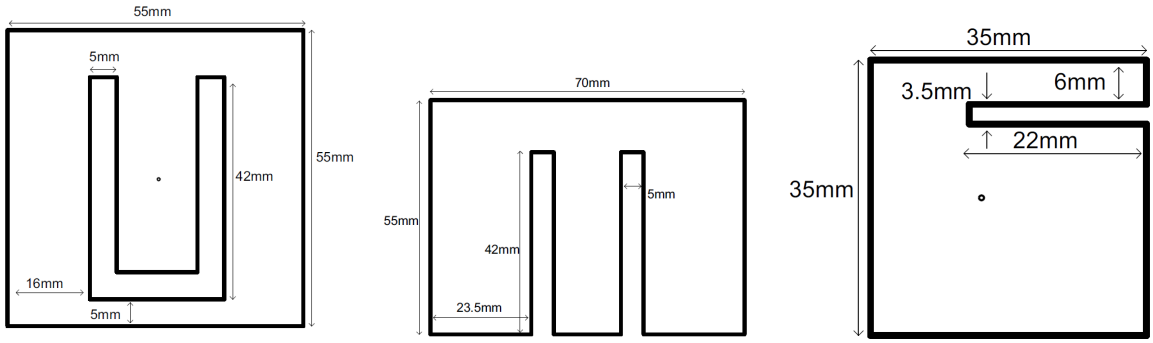

(a) U-slot. (b) E-slot. (c) C-slot.

Figure 5.6: Microstrip patch slotted techniques proposed in [4].

Thicker Substrate

As stated before, the main bandwidth constrain is the dielectric substrate. The thin dielectric substrate induces the bandwidth reduction [42].

Additionally, a dielectric with low permittivity provides improved bandwidth. Therefore, the intuitive approach is to use a thick substrate with low dielectric constant. However, thick substrate induce spurious feed radiation (increasing the power losses) and the low dielectric constant leads to larger antenna surfaces, according to Equation 5.4 and Equation 5.5. Also, the available commercial substrates have restrict heigh ($0.003\lambda_0$ to $0.05\lambda_0$) and permittivity (2.2 to 12). Solutions to obtain wideband microstrip patch antennas based onto the substrate height have been proposed, such as the multi-layer dielectric presented in [43].

Combining some of the previous mentioned techniques is also a possibility to overcome the narrow microstrip patch antenna bandwidth. Moreover, they might also induce antenna gain.

5.3 Antenna Design

The following section focuses on the patch antenna design to employ as D-TV receiver. Among the feed techniques previously presented, probe feed is used in the actual work. Beyond the previously mentioned advantages, this technique will allow, in the future, directly connect the antenna with the rectifier circuit, without need for SMA connectors. This results in a smaller system that, in practical situations, becomes capable to fit in tight areas and produces lower visual impact.

The main goals to take into account during the antenna design are as follow:

- Bandwidth – the antenna should maintain a good performance within the entire D-TV channel 56. Along this work, the -10 dB return loss (S_{11}) will be used as bandwidth metric. Hence, $S_{11}(dB)$ needs to remain below -10 dB at least between 750 to 758 MHz. However, it is important to obtain an higher bandwidth to deal with possible practical deviations.

- Gain – increasing the antenna gain, more power will be delivered to the rectifier and, consequently, the EH system performance increases. This is especially beneficial at low input power levels and aims to improve the operating range of the system.

- Input impedance – to promote the impedance matching between antenna and rectifier, their input impedances are designed to 50 Ohm, taking advantage of the easy adaptation provided by the probe feed technique.

- Low cost – the antenna, as well all the system, is intended to be low cost. The antenna costs are mainly defined by the dielectric substrate employed and the manufacturing process. Thus, maintaining the low profile associated to the microstrip patches and employ a cheaper commercial dielectric substrate is the key to reduce the costs.

Regarding the dielectric substrate, the choice was the FR-4, mainly due to the low cost and wide availability. Also, the dielectric constant ($\varepsilon_r = 4.3$) is a compromise between a good antenna performance and size: not too small in order to have an antenna with lower dimensions and not too large in order to have wider bandwidth.

The FR-4 dielectric substrate main characteristics are presented in Table 5.1. The available dielectric thickness is 1.6 mm, which is quite challenging due to the small height compared to the considered wavelength ($\lambda_0 = 400mm$), resulting in a narrow bandwidth as previously mentioned.

As antenna design tool, the CST Microwave Studio is employed – a finite difference time domain electromagnetic simulator.

5.3.1 Antenna Simulations – Proceedings and Results

Until the final proposed antenna, other approaches were considered. Hence, the following analysis aims to evidence and justify the considered sequential steps. The main

Dimension	Description	Value
ε_r	dielectric constant	4.3
tan δ	loss tangent	0.025
h	thickness	1.6

Table 5.1: Main characteristics of the FR-4 dielectric substrate.

performance results of each one are exhibited and analysed. Additionally, parametric studies relative to some microstrip antenna dimensions are provided. This studies intends to cover with some detail the behaviour of the considered configurations and then make a reliable choice in their dimensions.

The three main steps along the design procedure were: (A) firstly, a basic microstrip patch antenna is presented and analysed; (B) Secondly, rectangular slots shapes onto the microstrip patch are suggested; (C) Finally, a microstrip stacked patch with one parasitic element is analysed, resulting in the final proposed antenna.

Basic Configuration Patch

As starting point, the basic configuration patch, as shown in Figure 5.2, is suggested. Its dimensions were initially established according to the equations presented in [35]. However, a slight resonance frequency deviation is verified.

Theoretically, L affects the resonance frequency and both W and $y0$ the adaptation. In fact, with small changes in the dimensions was verified that they are all related. Along with W and $y0$ changes, not only the adaptation is affected, but also the resonant frequency is shifted, however in a much lower scale than the shift caused by L. Still, to correct the resonance shift, a manual small adjust would be enough. Although, to obtain the best bandwidth performance and the correct resonance frequency, optimization is a good solution. Therefore, an optimization with 754 MHz resonance frequency, 8 MHz bandwidth and 50 Ohm input impedance as goals is made.

After the optimization, 5.4 MHz bandwidth at 754 MHz is established, which constitutes an improvement of 2 MHz and results in the correction of the resonant frequency. The basic microstrip patch antenna has 3.1 dBi maximum gain, according to Figure 5.7.

Relative to the dimensions, the basic microstrip has: $L = 93.5$ mm; $W = 93.5$ mm; $y0 = 25.5$ mm. The ground plane was defined as a square of 187×187 mm.

Although the optimization improvements, it's verified the microstrip patch bandwidth constrains, as expected due to the small dielectric substrate height compared with the wave-length. A 5.4 MHz bandwidth is quite narrow and don't cover the entire channel 56 from the Portuguese D-TV. Thus, the slotted microstrip patch will be following presented to overcome this problem.

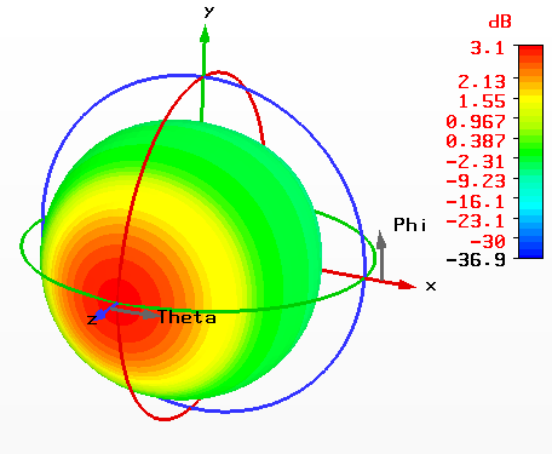

Figure 5.7: Basic microstrip patch antenna radiation pattern.

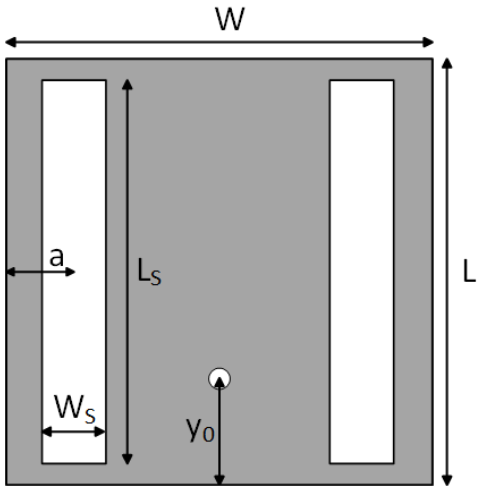

Figure 5.8: Configuration of the slots in the patch antenna.

Slots Technique

As first attempt to improve the basic microstrip patch antenna bandwidth, is proposed the introduction of slots onto its surface. The reported bandwidth improvements in literature with this technique as well non extra area required, were the main reasons for this choice.

As mentioned before, there are many slot shapes that have been proven useful to enhance antenna bandwidth. During the design process were tested some of them, however, introduction of two rectangular slots has provided a easy solution, with the quite good bandwidth improvement. The microstrip patch antenna with etched rectangular slots is exhibited in Figure 5.8, where were identified the adopted parameter dimensions designation. It should be noticed that slots are vertically centred in relation to the microstrip patch.

After obtaining a set of dimensions which has allowed the slots resonant frequency to become closer to the first and main resonant frequency, proceeded to a parametric study about the length and width slot dimensions and their horizontal position. This parametric study is shown in Figure 5.9, where both imaginary and real impedance components are used to evaluate the dimensions effect into the resonant frequency as well adaptation. Thus, Figure 5.9a exhibits the slots width W_S response, Figure 5.9b focuses into the slots horizontal position a and, finally, Figure 5.9c in the slots length L_S.

In general, it's clear that slot parameters have a significant impact in the second antenna resonance. Despite W_S causes also a shift in the main resonance, both a and L_S mainly affects the second antenna resonance. It also worth mention, that this dimensions are quite sensitive. A few millimetres change in them causes a significantly impedance deviation. For example, according to Figure 5.9a, changing W_S from 3 to 5.2 mm induce a second resonance shift around 27 MHz (from 785 MHz to 758 MHz) or, according to Figure 5.9b, moving the slots 1.7 mm towards the microstrip patch center ($a = 12$ mm to $a = 13.7$ mm) forces a shift in the second resonance of almost 20 MHz.

Moreover, Figure 5.9 also shows that with $W_S = 5.2$ mm, $a = 13.7$ mm and $L_S = 75$ mm the two resonant frequencies become closer to each other with improved adaptation (almost null imaginary component within 750 and 758 MHz) and, consequently, its possible to establish wider bandwidth.

With this slot configuration a bandwidth about 10 MHz is verified, about double the obtained with the basic configuration. However, there are yet two main limitations: the bandwidth, despite cover the entire 56 channel, is very tight and if a considerable simulation deviation occurs in practice the antenna becomes useless; there wasn't verified a gain enhancement, remaining similar to the obtained with the basic patch.

Therefore, a new attempt to obtain a better antenna performance is made with the stacked configuration, as following explained.

Stacked Patch

As consequence of the inappropriate performance results reached with the previous microstrip patch antennas configurations, is presented a new approach: a stacked antenna with one parasitic element and air gap between feeding and parasitic patches, as shown in Figure 5.5. Due to the substrate availability limitations and to keep the antenna low cost, the upper patch is made with the same substrate as the bottom – FR-4. In fact, to obtain improved performance the feeding patch should have higher ε_r than the parasitic, reducing the coupling in the later and, therefore, increasing the bandwidth, as proposed in [38] and [39]. Hence, in order to reduce the coupling larger air gap distance might be required in the present work.

The goal is to take advantage of both slotted and stacked techniques. However, small changes in one of the dimensions usually requires changes in the others. Therefore, to simplify the stack performance study according to its dimensions and air gap distance, it's taken as feeding patch the initial basic patch.

Firstly, it was verified that the upper patch dimensions (length L_P and width W_P)

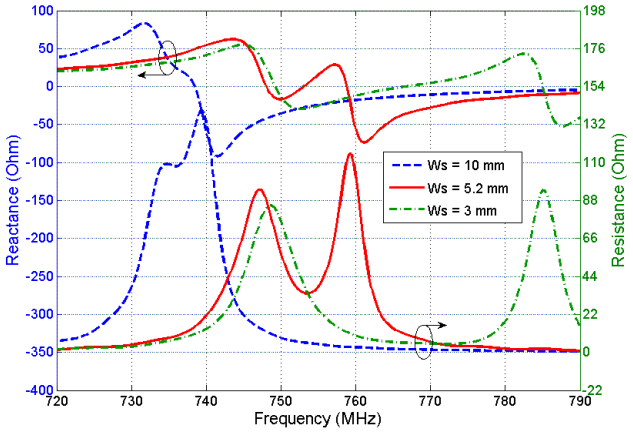

(a) W_S parameter variation.

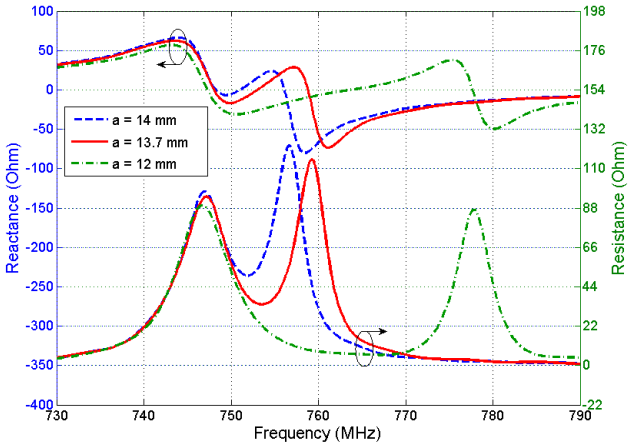

(b) a parameter variation.

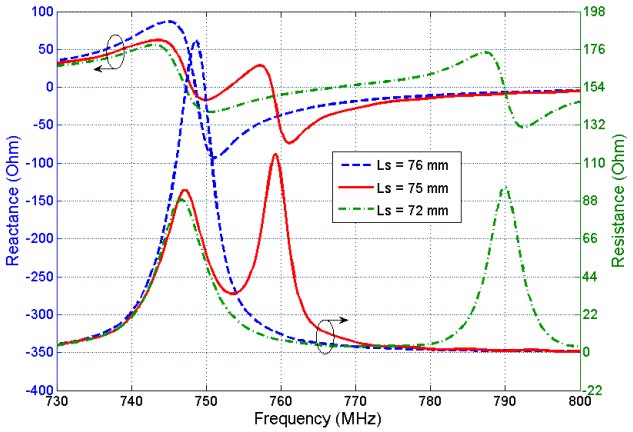

(c) L_S parameter variation.

Figure 5.9: Slotted microstrip patch imaginary and real impedance components.

produces small changes in the antenna performance, for a certain air gap, H. Both L_P and W_P are proportional to the feeding patch L and W, respectively, by a multiplicative factor (mf): $W_P = mf \times W$ and $L_P = mf \times L$. This dimensions are exhibited in Figure 5.10. Through simulation analysis, mf is set to 1.45.

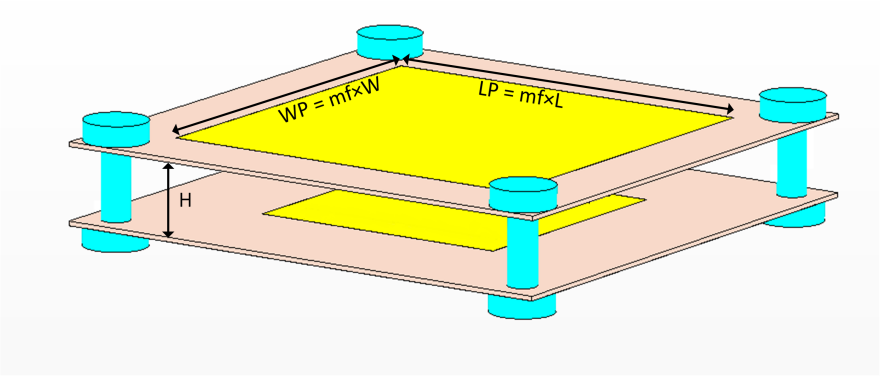

Figure 5.10: Stacked patch antenna – parasitic dimensions.

Regarding the air gap, Figure 5.11 presents the simulation results of the input return loss for various values of air gap distance, H, between the patches. In order to correct the shift in the resonant frequency and obtain the wider bandwidth, each change in H is followed by a slight adjustment in the patches dimensions, maintaining the mf value. Thus, according to Figure 5.11, the minimum air gap considered $(0.025\lambda_0)$ corresponds to the minimum bandwidth and increasing it results in an wider bandwidth.

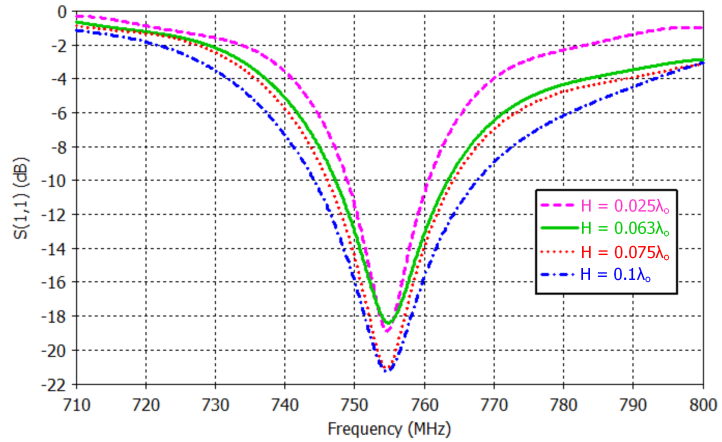

Figure 5.11: Return loss of the stacked patch antenna for different H values.

Additionally, the air gap also affects the antenna gain. Once again, as H increases a gain improvement is verified. Figure 5.12 presents the gain obtained with both lower (Figure 5.12a) and higher (Figure 5.12b) H values. To summarize, Table 5.2 shows the bandwidth and gain obtained for each air gap. It should be noted, that even the stacked

patch with the lower tested H presents improved bandwidth and gain than the basic patch antenna.

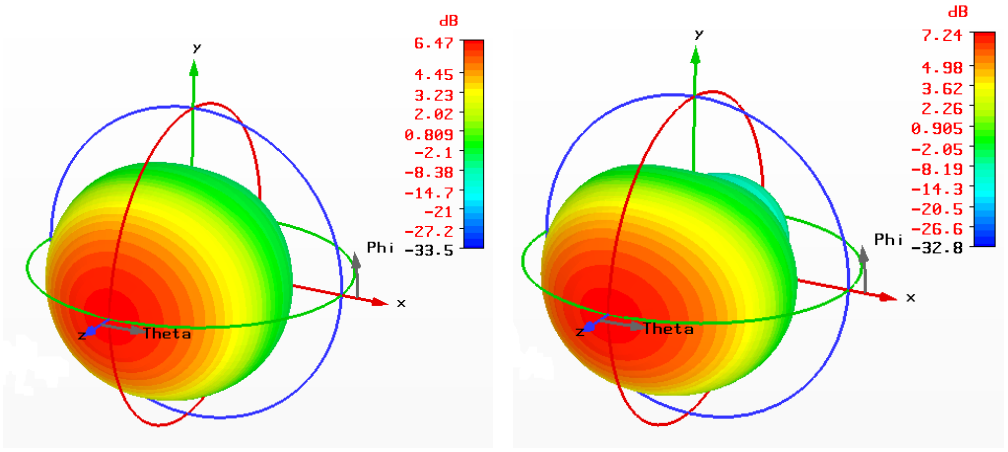

(a) $H = 0.025\lambda_0$. (b) $H = 0.1\lambda_0$.

Figure 5.12: Stacked antenna radiation pattern for different H values.

H (m)	BW (MHz)	G (dBi)
$0.025\lambda_0$	12	6.47
$0.063\lambda_0$	16	7.16
$0.075\lambda_0$	18	7.19
$0.1\lambda_0$	24	7.24

Table 5.2: Stacked antenna bandwidth and gain variation as function of H.

Proposed Antenna

In the proposed antenna, both slot and parasitic stacked techniques are employed. The bottom patch with slots has the same configuration as presented in Figure 5.8. However, the introduction of the parasitic stack forced a new adjustment on the slot dimensions to maintain both resonance frequencies within the desired bandwidth.

Despite shown before that higher air gap produces improved results, due to physical limitations in the available spacers and screws required to fix the air distance, H is set to 25 mm ($\approx 0.063\lambda_0$). Still, this air gap agrees with the ones proposed in the literature, as previously mentioned. Both spacers and screws are made of nylon.

Thus, the proposed antenna has the dimensions present in Table 5.3. Simulation predicts 20.7 MHz bandwidth, an enhancement around 15 MHz relative to the basic initial

microstrip patch. This results are plotted in Figure 5.13, as well the slotted patch input reflection coefficient. Hence, the bandwidth improvements between successive configurations becomes clear. Attending to the gain, is expected to obtain 6.9 dBi with this proposed antenna. This result is also a significant improvement towards the gain of both basic and slotted patch antennas (an increase around 4 dB).

	Description	Dimension (mm)
L	Length of the feeding patch	90.8
W	Width of the feeding patch	91.5
y_0	Location of the probe feed	6.3
L_P	Length of the parasitic patch	131.7
W_P	Width of the parasitic patch	132.7
L_S	Length of the slots	81
W_S	Width of the slots	11.7
a	Location of the center of the slots	9.3
H	Distance between the patches	25
mf	Multiplicative factor	1.45

Table 5.3: Proposed antenna dimensions.

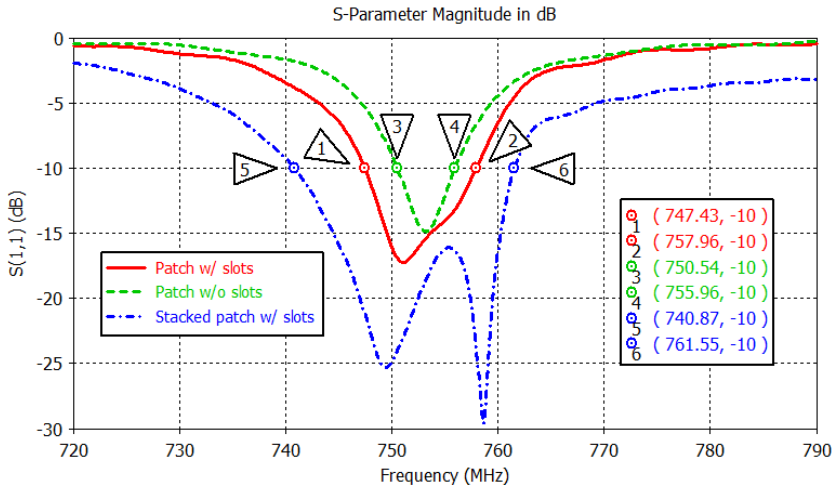

Figure 5.13: Simulated return loss of the proposed antenna, slotted and basic patch.

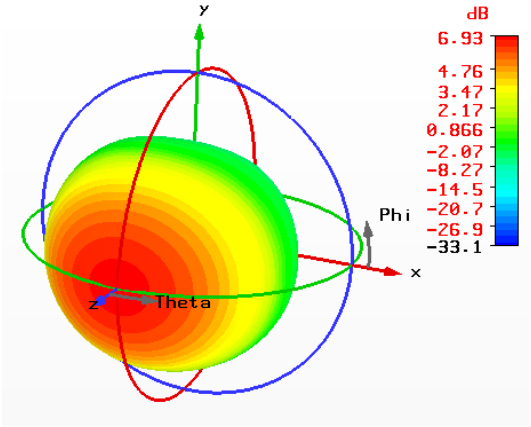

Figure 5.14: Radiation pattern of the proposed antenna.

5.4 Antenna Measurements

A perspective view of the implemented antenna is shown in Figure 5.15. To evaluate the bandwidth, the input reflection coefficient is measured in the VNA. The measured S_{11} is presented in Figure 5.16 and compared with the expected through simulation. The antenna is resonant at 776.5 MHz, a shift about 20 MHz the predicted. This deviation could be justified by uncertainty of FR-4 permittivity – a poor characterized dielectric. However, a good agreement between measured and simulated bandwidth is reached (22.5 MHz and 20.7 MHz, respectively).

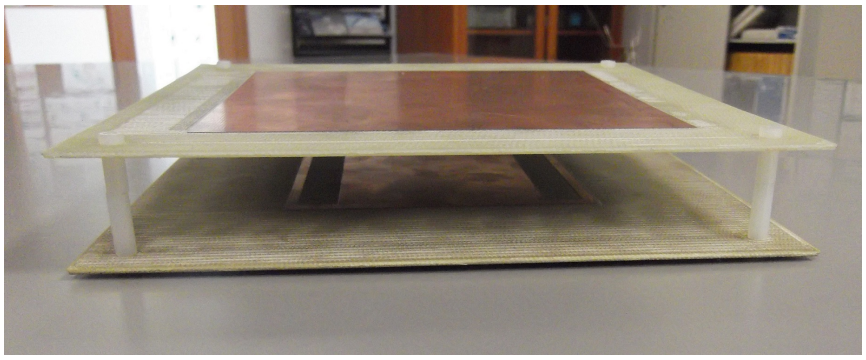

Figure 5.15: Implemented antenna.

To overcome the resonance frequency deviation, the H parameter was tested for different values as shown in Figure 5.17. It can be noticed that as the feeding patch gets closer the parasitic patch, the resonance frequency decreases. In fact, by reducing the H the coupling between them increases and the larger patch (parasitic) forces the resonance frequency to decrease. Another important conclusion to take from Figure 5.17 is that the distance between patches decrease is followed with a slight reduction in the bandwidth, as expected with previously simulated results.

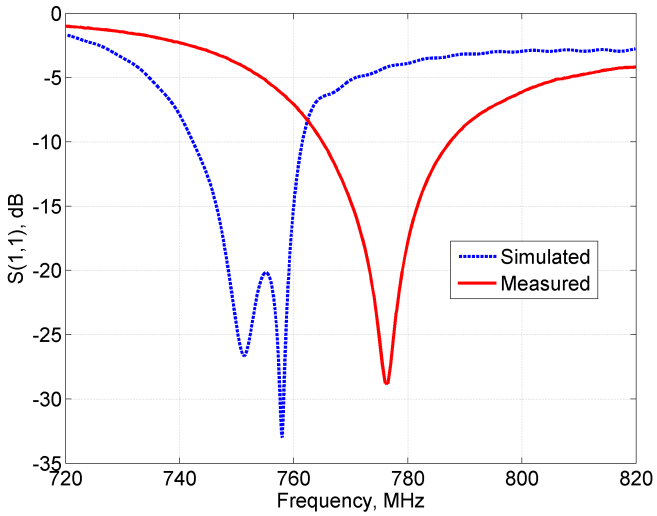

Figure 5.16: Measured and simulated S_{11}.

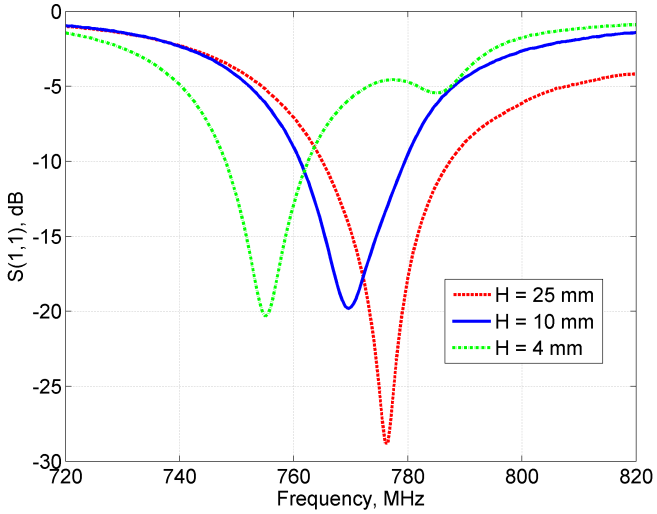

Figure 5.17: Return loss of the implemented antenna for different distances between patches.

As conclusion, despite the discrepancy in the resonant frequency, the air gap distance adjustment resulted in an antenna with the required bandwidth and frequency of operation to use as Portuguese D-TV receiver. This is accomplished with $H = 4$ mm and the corresponding bandwidth is 14.5 MHz.

Chapter 6

System Validation

In this chapter is evaluated the performance of the RF-to-DC system. For this purpose, one of the developed rectifiers is connected to the antenna and measurements with the real D-TV signal are performed. As proof of concept, these measurements are made only with the voltage doubler as rectifier, due to its enhancement performance compared to the shunt and series diode configuration, as analysed in Chapter 4. The microstrip patch antenna developed and presented in Chapter 5 will be used as receiver antenna. The measurements take place around the Aveiro central D-TV transmitter. The system performance will focus on the rectifier output DC voltage.

6.1 Measurements

The map presented in Figure 6.1 marks the locations from A to O where the measurements take place. As shown, all the markers are located around the Aveiro centre D-TV transmitter, indicated in the map as Tx. To proceed with the measurements, the antenna and the voltage doubler are connected to each other and a multimeter is then connected to the output of the rectifier to obtain the DC voltage across the load.

The output DC voltage obtained in each marker is presented in Table 6.1. Also, in Table 6.1 are summarized the distance of each marker to the D-TV transmitter and an empirical estimation of the altitude relative to the transmitter antenna[1]. Distance and altitude are important to take some conclusions further ahead. Furthermore, in the measurements presented in Table 6.1, the EH system and the transmitter were always in line of sight, otherwise it was verified that the output DC voltage obtained is minor. As remaining note, the output DC voltage isn't most of the times a fixed value. It keeps changing according to the receiver power that, in turn, changes mainly with small motions of the EH system. Therefore, Table 6.1 presents the maximum DC voltage obtained with the multimeter in

[1]high – measure location is at the same altitude as the transmitter; average – measure location is around half the altitude of the transmitter; low – measure location is at a very small altitude compared to the transmitter.

each marker. In these conditions, was obtained the higher DC voltage at marker B (0.91 V) and the lower at marker A (0.08 V).

To prove Table 6.1 results, Figure 6.2 shows some of these measurements associated with the respective map marker.

Besides output DC voltage, efficiency is also a key in RF-to-DC evaluation performance. However, with these input power deviations it is hard to obtain an accurate relation between input power and output voltage to then compute the efficiency. To overcome this problem the receiver antenna was fixed on the marker B floor and, despite not being located in the best position, the received power was measured with the SA and then the rectifier was connected and the DC output voltage was obtained. Figure 6.3a shows the received power obtained with the SA and Figure 6.3b presents the respective voltage doubler DC output voltage. As consequence, the efficiency is 63.2%, obtained through Equation 2.3.

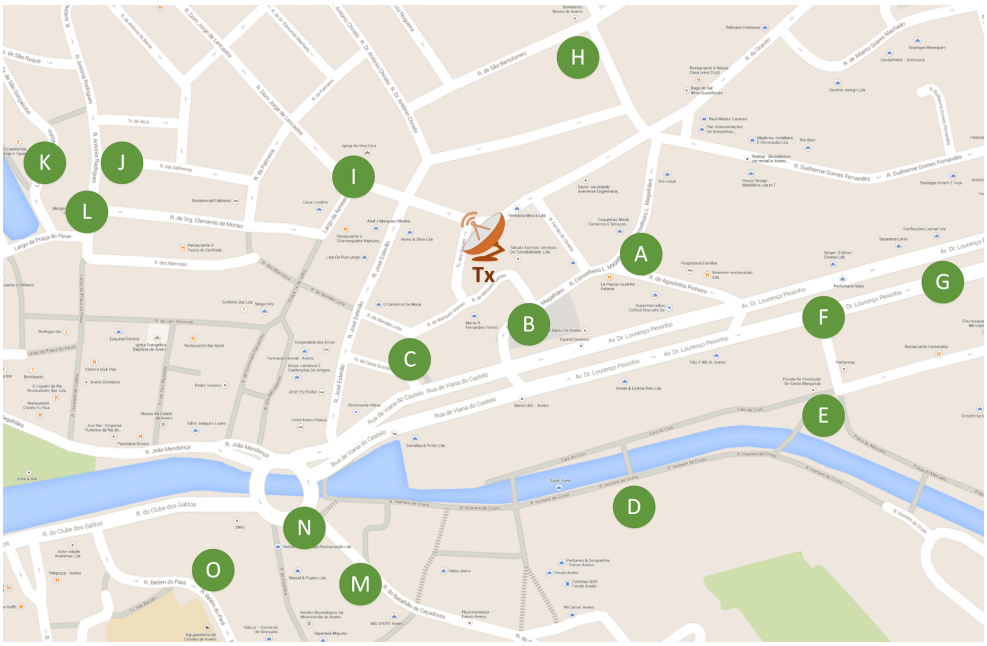

Figure 6.1: Locations of the measurements and D-TV transmitter in Aveiro city.

Location Marker	Distance to transmitter (m)	Altitude	Maximum V_{DC} (V)
A	100	high	0.08
B	55	high/average	0.91
C	70	low	0.32
D	190	average	0.56
E	235	low	0.12
F	215	low	0.17
G	270	low	0.19
H	140	low	0.36
I	90	low	0.49
J	230	low	0.45
K	270	average/low	0.6
L	240	low	0.33
M	210	low	0.21
N	190	low	0.14
O	240	low	0.39

Table 6.1: Output DC voltage around Aveiro D-TV transmitter.

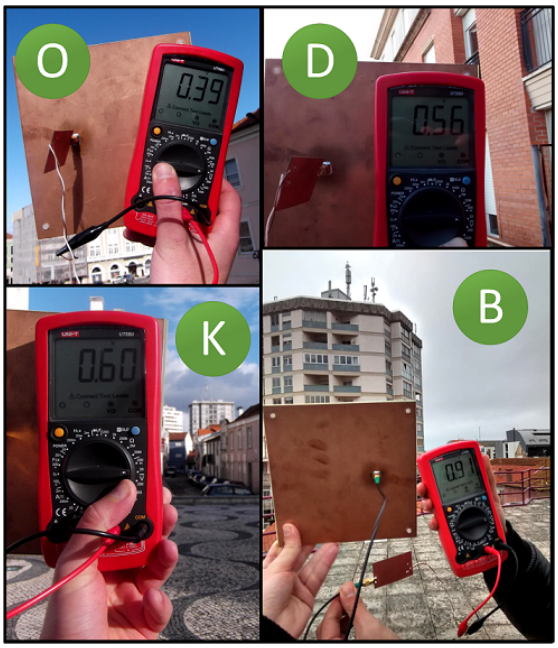

Figure 6.2: Output DC voltage around D-TV transmitter at four different locations.

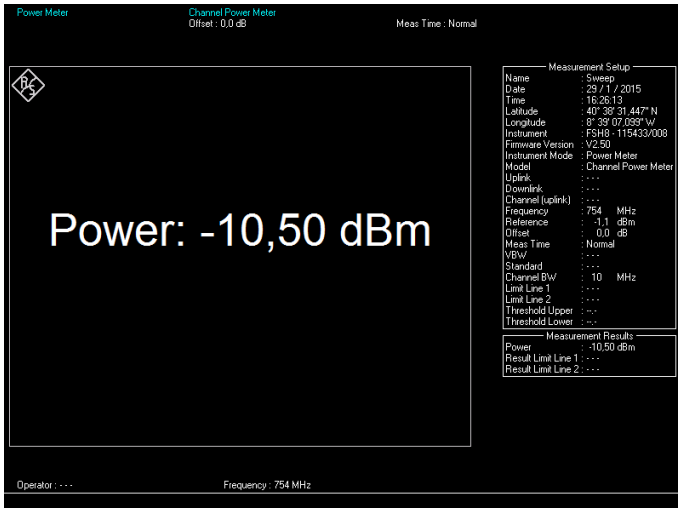

(a) Received power.

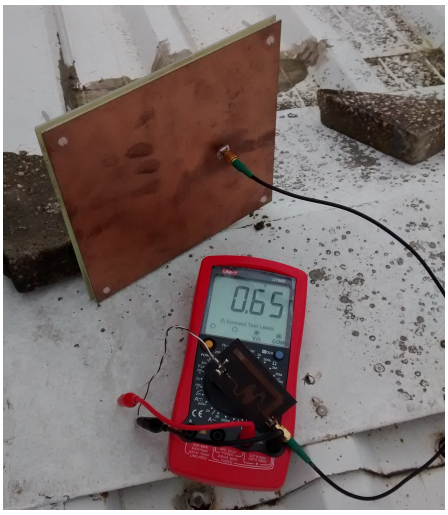

(b) Output DC voltage.

Figure 6.3: Measures at marker *B*.

6.2 Analysis

As mentioned in Section 6.1, line of sight between the transmitter and EH system is required to obtain the expected EH system performance. Also, attending to Table 6.1, distance and altitude play an important role. The relation between distance and performance is easily explained by the basic Friis transmission equation (Equation 2.1) shown in Chapter 1 – path loss is proportional to the square distance between transmitter and receiver. Nevertheless, this equation assumes that transmitter antenna has the same gain in all directions and does not take into account the altitude difference between transmitter and receiver.

The minimum DC voltage with line of sight was found at marker *A* and it was a priori an unexpected value. In fact, due to its proximity to the transmitter and high altitude the odds were to obtain the best performance among all the other markers measures. However, spectrum measurements at *A* has shown a real poor D-TV signal. There might be a reasonable explanation for the occurrence: since the measures at marker *A* were made at the top of a building with approximately the same altitude than the transmitter and they are the highest buildings in the center of the city, it's reasonable to assume that transmitter antennas are slightly tilted in a way that the maximum gain is in the lowest buildings direction.

Apart marker *A* measures, the remaining results are roughly according with the expected and, as already mentioned, marker *B* presents the higher output voltage (0.91 V). This is mainly due to the transmitter proximity but also due to fact that marker *B* measures were made on the top of a building with average altitude (probably in the maximum gain transmitter direction) and with few obstacles, reducing the signal reflections.

Both *G* and *K* markers are located at around 270 meters. However, the output DC

voltage obtained in each one are quite different: 0.19 V at G and 0.6 V at K. The slightly higher altitude of measure at marker K or the fact there is more obstruction at marker G due to the high density buildings in the surroundings might result in less power losses in the path and then improve the RF-to-DC response.

Other similar cases as the previous are the measures at markers D and N. Again, they are both at the same distance from the transmitter, however, marker D measures have shown improved results and the explanations of the previous case are also valid for this one.

In contrast to the previous cases, markers L and O are at the same distance from the transmitter and roughly at the same altitude and the output DC voltage in each one are very similar: 0.33 V at L and 0.39 V at O. On the other hand, for example, markers E, F and M are near to the transmitter and the obtained voltage was lower in all of them. This emphasis the fact there are more factors than distance that influence the system performance.

The 63.2% voltage doubler efficiency that was possible to measure at marker B corresponds to an input power of -10.5 dBm, as presented in Section 6.1. The voltage doubler measurements made with the signal generator presented in Section 4.3.1 indicate an efficiency around 56.5% for the same input power level. The difference between the laboratory and Aveiro city measurements is the excitation signal. While laboratory measurements were made with a sine-wave, at Aveiro center was used the real D-TV signal. This improvement results from the fact that D-TV signal has a certain PAPR higher than the one from a sine-wave that, as previously explained, increases the conversion efficiency. Thus, it is proved the feasibility of the proposed energy harvesting system.

Chapter 7

Conclusions and Future Work

The main goal of the project was to design a system responsible for collecting electromagnetic energy that takes advantage of the high amount of D-TV transmitters in Portugal and, consequently, its wide-reaching. Thus, the system should present high efficiency at low input power levels to be able to power up low-power devices. Furthermore, along the work were evaluated different solutions to rectify the RF into DC power and was provided an overview into the strategy to follow in order to design the respective circuits with the suitable performance.

Therefore, the three rectifier circuits proposed along this work were designed to properly operate under weak power signals through a careful analysis of their elements. These circuits have shown an high efficiency at low-power conditions – around 54% with a single-tone excitation and 63.2% with the D-TV signal for -10.5 dBm in both cases. Thus, it was proved the rectifiers feasibility and verified the performance enhancement with the D-TV signal excitation. Regarding the microstrip patch antenna designed to collect the electromagnetic energy, the effort in improving its bandwidth and gain has resulted in an antenna with the desired performance. The proposed solution has provided a bandwidth increase of 4 times the expected to obtain with the first approach. Moreover, the antenna design also constitutes a good study and presents the strategy followed to improve these microstrip patch limitations.

There are many work regarding RF-to-DC conversion with considerable efficiencies. Although, most of them are characterized for higher input power levels, which becomes useless for energy harvesting applications. Hence, this work is differentiated by obtaining a similar performance at lower power levels with a low cost antenna and rectifier, resulting in a quite good contribution for energy harvesting.

Despite the improved performance of the system, there are some considerations that can be taken as future work to attempt to increase it even more and also to reduce its dimensions. Firstly, the matching network required to match the rectifier input impedance to the antenna has shown to produce significant losses relative to an ideal matching. Thus, should be considered a solution that discards its need and, of course, provides the required matching between them. Secondly, the antenna is too large comparing to the rectifier, which increases the overall system dimensions and can constitute a limitation for some

applications. Therefore, it also should be analysed the possibility to reduce the antenna dimensions or employ a smaller one to enable the system to fit in tight areas. Although, it's important to keep its performance to guarantee the proper system functionality.

At large scale, the future work should go through design and developing a practical application to employ the EH system. One main application is a Wireless Sensor Network (WSN), taking advantage of the amount of low-power sensors available and turning them into self-sustainable devices. Another possible application is to create an hybrid system by integrating the D-TV EH with another EH source, such as solar radiation. This would result in a much more reliable system that would be able to power up higher consumption devices.

Bibliography

[1] P. Glaser, "Method and apparatus for converting solar radiation to electrical power," 1973.

[2] H. Sun, Y. X. Guo, M. He, and Z. Zhong, "Design of a high-efficiency 2.45-GHz rectenna for low-input-power energy harvesting," *IEEE Antennas and Wireless Propagation Letters*, vol. 11, pp. 929–932, 2012.

[3] V. Marian and B. Allard, "Strategy for microwave energy harvesting from ambient field or a feeding source," *Power Electronics, IEEE Transactions*, vol. 27, no. 11, pp. 4481–4491, 2012.

[4] S. Bhardwaj and Y. Rahmat-Samii, "C-shaped, E-shaped and U-slotted patch antennas: Size, bandwidth and cross-polarization characterizations," *Antennas and Propagation (EUCAP), 2012 6th European Conference on*, pp. 1674–1677, 2012.

[5] N. Tesla, "Apparatus for Transmission of Electrical Energy," 1990.

[6] N. Shinohara, "Wireless Power Transmission for Solar Power Satellite (SPS) (Second Draft by N . Shinohara).".

[7] W. C. Brown, "Electronic and Mechanical Improvement of the Receiving Terminal of a Free-space Microwave Power Transmission System," *NASA contractor report for National Aeronautics and Space Administration*, vol. 135194, p. 158, 1977.

[8] W. Brown and J. Triner, "Experimental Thin-Film, Etched-Circuit Rectenna," *Microwave Symposium Digest, 1982 IEEE MTT-S International*, pp. 185–187, 1982.

[9] F. Zhang, Y. Zhang, J. Silver, and Y. Shakhsheer, "A Batteryless 19uW MICS/ISM-Band Energy Harvesting Body Area Sensor Node SoC," *Solid-State Circuits Conference Digest of Technical Papers (ISSCC), 2012 IEEE International*, vol. 46, pp. 288–289, 2012.

[10] W. Brown, "The history of wireless power transmission," *Solar energy*, vol. 56, no. 1, pp. 3–21, 1996.

[11] D. M Pozar, *Microwave Engineering, 3rd.* 2005.

[12] S. S. Mohammed, K. Ramasamy, and T. Shanmuganantham, "Wireless Power Transmission - A Next Generation Power Transmission System," *International Journal of Computer Applications*, vol. 1, pp. 102–105, 2010.

[13] A. Boaventura, A. Collado, N. Carvalho, and A. Georgiadis, "Spatial Power Combining of Multi-Sine Signals for Wireless Power Transmission Applications," *Microwave Theory and Techniques, IEEE Transactions*, vol. 62, pp. 1022–1030, 2014.

[14] C. Lo, Y. Yang, and C. Tsai, "Novel wireless impulsive power transmission to enhance the conversion efficiency for low input power," *Microwave Workshop Series on Innovative Wireless Power Transmission: Technologies, Systems, and Applications (IMWS), 2011 IEEE MTT-S International*, pp. 55–58, 2011.

[15] ANACOM, *Quadro nacional de atribuição de frequências*. Edição 2009/2010.

[16] "TDT – Televisão Digital Terrestre." `http://tdt.telecom.pt/`. [Online; accessed June-2015].

[17] "ANACOM, Rede de frequência única - canal 56." `http://www.anacom.pt/render.jsp?contentId=1021427#.VY699UZJfEY`. [Online; accessed March-2015].

[18] W. Brown, "An experimental low power density rectenna," *1991 IEEE MTT-S International Microwave Symposium Digest*, 1991.

[19] A. Boaventura, A. Collado, N. Carvalho, and A. Georgiadis, "Optimum behavior: Wireless power transmission system design through behavioral models and efficient synthesis techniques," *Microwave Magazine, IEEE*, pp. 26–35, 2013.

[20] G. A. Vera, A. Georgiadis, A. Collado, and S. Via, "Design of a 2.45 GHz rectenna for electromagnetic (EM) energy scavenging," in *2010 IEEE Radio and Wireless Symposium, RWW 2010 - Paper Digest*, pp. 61–64, 2010.

[21] A. Collado and A. Georgiadis, "Improving wireless power transmission efficiency using chaotic waveforms," *2012 IEEE/MTT-S International Microwave Symposium Digest*, pp. 1–3, 2012.

[22] B. Franciscatto and V. Freitas, "High-efficiency rectifier circuit at 2.45 GHz for low-input-power RF energy harvesting," *Microwave Conference (EuMC), 2013 European*, pp. 507–510, 2013.

[23] A. Georgiadis, A. Collado, S. Via, and C. Meneses, "Flexible hybrid solar/EM energy harvester for autonomous sensors," *IEEE MTT-S International Microwave Symposium Digest*, pp. 6–9, 2011.

[24] C. Mikeka, H. Arai, A. Georgiadis, and A. Collado, "DTV band micropower RF energy-harvesting circuit architecture and performance analysis," in *2011 IEEE International Conference on RFID-Technologies and Applications, RFID-TA 2011*, pp. 561–567, 2011.

[25] Avago Technologies, *HSMS-285x Series - Surface Mount Zero Bias Schottky Detector Diodes*, 4 2009.

[26] M. Muramatsu, H. Nishiyama, and H. Koizumi, "Effects of parasitic circuit elements in RF energy harvesting circuit," *Sustainable Energy Technologies (ICSET), 2012 IEEE Third International Conference on*, vol. 7, pp. 18–22, 2012.

[27] J. Guo, H. Zhang, and X. Zhu, "Theoretical Analysis of RF-DC Conversion Efficiency for Class-F Rectifiers," vol. 62, no. 4, pp. 977–985, 2014.

[28] S. A. Maas, *Nonlinear Microwave and RF Circuits*. 2nd ed., 2003.

[29] A. Mabrouki, M. Latrach, and Z. Sayegh, "Design and Experiment of RF Rectifiers for Wireless Power Transmission," *Microwave Symposium (MMS), 2013 13th Mediterranean*, vol. 1, pp. 0–3, 2013.

[30] C. Valenta and G. Durgin, "Harvesting wireless power: Survey of energy-harvester conversion efficiency in far-field, wireless power transfer systems," *Microwave Magazine, IEEE*, no. May, 2014.

[31] Avago Technologies, *HSMS-282x - Surface Mount RF Schottky Barrier Diodes*, 11 2014.

[32] Avago Technologies, *HSMS-286x Series - Surface Mount Microwave Schottky Detector Diodes*, 8 2009.

[33] Skyworks, *SMS7630 Series - Surface Mount Mixer and Detector Schottky Diodes*, 8 2014.

[34] Rogers Corporation, "RT/duroid 5870/5880 High Frequency Laminates." 2015.

[35] C. Balanis, *Antenna theory: Analysis and design*. 3th ed., 2005.

[36] K. Carver and J. Mink, "Microstrip antenna technology," *IEEE Transactions on Antennas and Propagation*, vol. 29, pp. 2–24, 1981.

[37] P. B. Parmar, B. J. Makwana, and M. a. Jajal, "Bandwidth Enhancement of Microstrip Patch Antenna Using Parasitic Patch Configuration," *2012 International Conference on Communication Systems and Network Technologies*, pp. 53–57, May 2012.

[38] K. L. Chung and A. S. Mohan, "A Systematic Design Method to Obtain Broadband Characteristics for Singly-Fed Electromagnetically Coupled Patch Antennas for Circular Polarization," *IEEE Transactions on Antennas and Propagation*, vol. 51, pp. 3239–3248, 2003.

[39] K. Chung and A. Mohan, "Design of stacked circular/quasi-elliptical patch array for broadband CP applications," *6th International SYmposium on Antennas, Propagation and EM Theory*, 2003.

[40] M. D. Sharma, A. Katariya, and R. Meena, "E Shaped Patch Microstrip Antenna for WLAN Application Using Probe Feed and Aperture Feed," *2012 International Conference on Communication Systems and Network Technologies*, pp. 66–70, May 2012.

[41] A. Munir, G. Petrus, and H. Nusantara, "Multiple slots technique for bandwidth enhancement of microstrip rectangular patch antenna," in *2013 International Conference on Quality in Research, QiR 2013 - In Conjunction with ICCS 2013: The 2nd International Conference on Civic Space*, pp. 150–154, 2013.

[42] D. Pozar, "Microstrip antennas," *Proceedings of the IEEE*, vol. 80, 1992.

[43] Z. Chen, T. See, and X. Qing, "Multi-dielectric layer multi-patches microstrip antenna for UWB Applications," *Wireless Technologies, 2007 European Conference on*, vol. 3, pp. 1019–1021, 2007.